7 Multiresolutional Wavelet Analysis

7.1 Introduction

Multiscale analysis based on wavelet analysis, being a very modern and extensively developed numerical technique in signal theory [147,148,380], even in probabilistic context [289], introduces the capability to analyse the composite systems with multiple geometrical scales, which is very realistic for most engineering composites (the scales of microdefects, interface, reinforcement and the entire structure). Nowadays, this technique is employed in porous materials modelling [104], general FEM and BEM solutions for boundary problems [119], in vibration analysis [235] as well as in crack detection and impact damages [293,331,343], for instance. Figure 7.1 below presents the MATLAB illustration of the signal that can be interpreted as the information about the variability of heterogeneous medium physical properties in time (and/or in space). It is seen how such a signal can be decomposed using discrete wavelet transforms on the partially homogeneous parameters on different levels [169,170]. After such a decomposition, the traditional or wavelet–based discrete numerical methods can be applied for computational physical modelling.

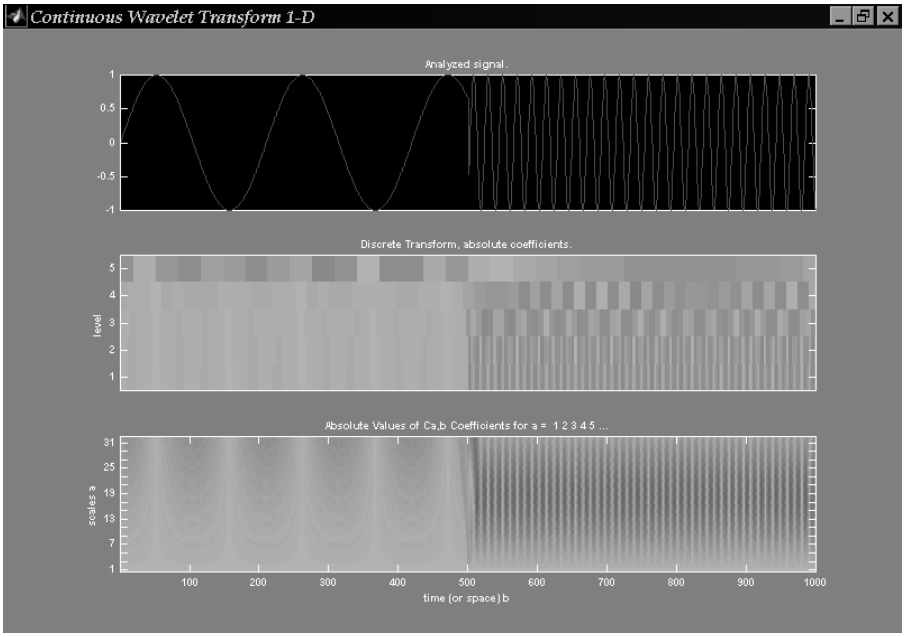

Figure 7.1. Discrete and continuous wavelet signal transform

The homogenisation method is still the most efficient way of computational modelling of composite systems. Usually it is assumed that there exists some scale relation between composite components and the entire system – two scales are introduced that are related by a scale parameter being some small real value tending most frequently to 0. An essential disadvantage of all these techniques is the impossibility of sensitivity analysis of composite homogenised characteristics with respect to geometrical scales relations.

Wavelet analysis became very popular in the area of composite materials modelling because of their multiscale and stochastic nature. The most interesting issue is composite global behaviour, which is more important than the multiphysical phenomena appearing at different levels of their complicated multiscale structure. That is why it is necessary to build an efficient mathematical and numerical multiresolutional algorithm to analyse composite materials and structures.

As is known, two essentially different ways are proposed to achieve this goal. First, the composite can be analysed directly using the wavelet decomposition–based FEM approach where the multiresolutional analysis can recover the material properties of any component at practically any geometrical level. The method leads to an exponential increase of the total number of degrees of freedom in the model – each new decomposition level increases this number.

Alternatively, a multiscale homogenisation algorithm can be applied to determine effective material parameters of the entire composite and next, to carry out the classical FEM or other related method–based computations. The basic difference between these two approaches is that the wavelet decomposition and construction algorithms are incorporated into the matrix FEM computations in the first method. The second method is based on the determination of the effective material parameters and Finite Element analysis of the equivalent homogeneous system, where the dimensions of the original heterogeneous and homogenised problems are almost the same. An analogous two methodologies had been known before the wavelet analysis was incorporated in engineering computations. However the homogenisation method assumptions dealing with the interrelations between macro– and microscales were essentially less realistic.

Considering the above, the aim of this chapter is to demonstrate the use of the wavelet–based homogenisation method in comparison with its preceding classical formulations. Effective material parameters of a periodic composite beam are determined symbolically in MAPLE and next, the temporal and spatial variability of thermal responses of homogenised systems are determined numerically and compared with the real structure behaviour. It is assumed here that material properties are temperature–independent, which should be extended next to the thermal–dependent behaviour. As is verified by the computational experiments, all homogenisation methods (classical and multiresolutional) give a satisfactory approximation of real heat transfer phenomena in the multiscale heterogeneous structure. The approach should be verified next for other types of composites as well as various physical and structural problems in both a deterministic and stochastic context. Separate studies should be carried out for the computer

implementation of wavelet analysis in the Finite Element Method programs and comparison with the multiscale algorithm.

Further, we demonstrate the application of the wavelet–based homogenisation method in comparison with its preceding classical formulation. Effective material parameters of the periodic composite beam are determined symbolically in MAPLE and next, the structural responses of the linear elastic homogenised systems are determined numerically and compared with the real structure vibrations. The eigenproblems for various combinations of the effective parameters are computed thanks to the specially adopted Finite Element Method computer code to determine the most efficient homogenisation method for the periodic multiscale composite. It is done for two–, three– and five–bay free supported periodic composite beams having their applications in the aerospace industry as well as in the modelling of bridge vibrations, for instance. As is verified by the computational experiments, the homogenisation methods (classical and multiresolutional) give a satisfactory approximation of the periodic composite beam eigenfrequencies. The approach should be verified next for other types of structures as well as for other structural problems in both deterministic and probabilistic context.

Wavelet analysis is an especially promising tool in the domain of composite materials. It enables: (1) constructing the multiscale heterogeneous structures using particular wavelets which has to perfectly reflect the manufacturing process, for instance, and (2) multidimensional decomposition of the spatial distribution of composite materials and physical properties by the use of the wavelets of various types defined in different scales (heat conductivity or Young modulus along the heterogeneous specimen). The first opportunity corresponds to the analysis of experimental results (image analysis of composite morphology), while the second reflects the theoretical and computational analysis.

Let us notice that the wavelet analysis introduces new meaning for the term *composite*. In the view of the analysis below we can distinguish homogeneous materials from composites using the following definition: *the composite material and/or structure is such a heterogeneous continuum in which material or physical properties are related in macro– and microscales by at least a single wavelet transform.* This definition extends traditional, rather engineering approach to composites where laminated or fibre–reinforced structures were considered (partially constant character of material characteristics) to those media with sinusoidal variability in one direction of these properties at least (see Figures 7.2–7.7 below). Figure 7.2 shows the spatial variability of the Young modulus using the following wavelet function [188]:

$$e(x) = e_0 + \sin\left(\frac{\pi x}{l}\right) + 0.1\sin\left(\frac{\pi 10^2 x}{l}\right) + 0.1\sin\left(\frac{\pi 10^4 x}{l}\right),\ l{=}10.$$

The next figures present the contributions of various scales to the macroscale elastic characteristic of the entire composite structure.

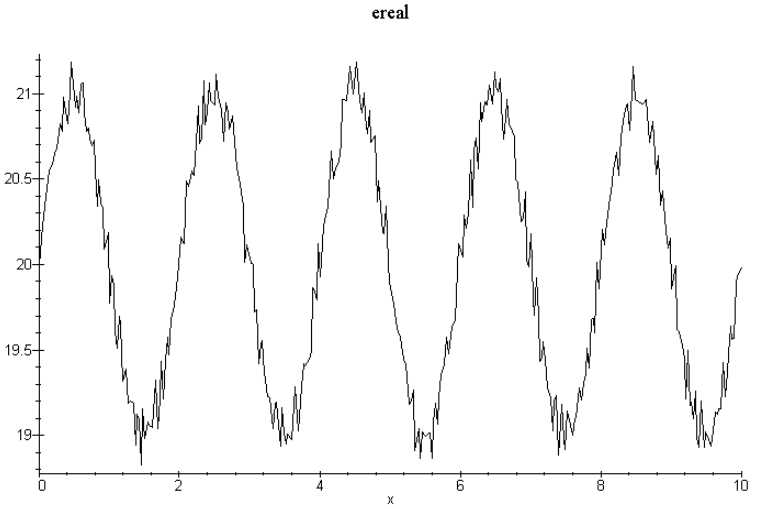

Figure 7.2. Distribution of the Young modulus in the real composite

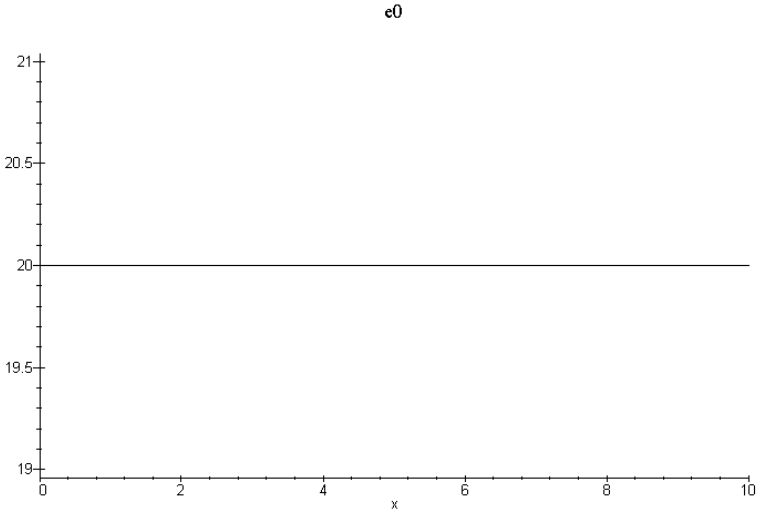

Figure 7.3. Zeroth order wavelet approximation of Young modulus in zeroth scale

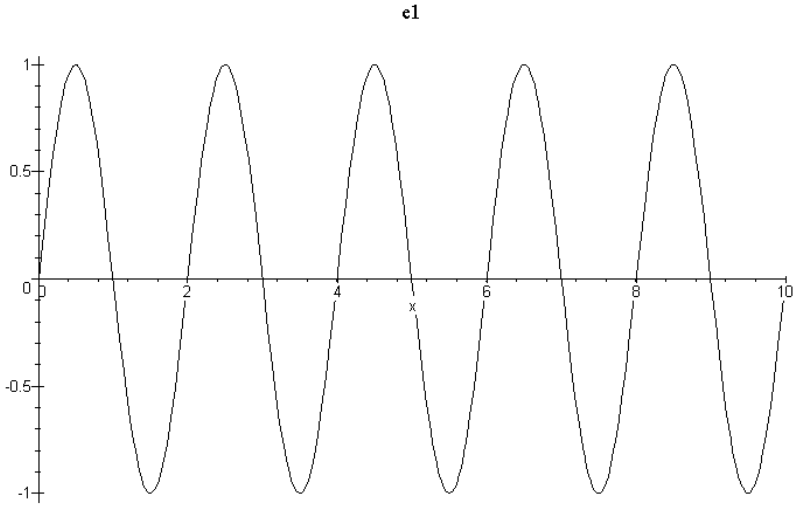

Figure 7.4. First order wavelet approximation of Young modulus in zeroth scale

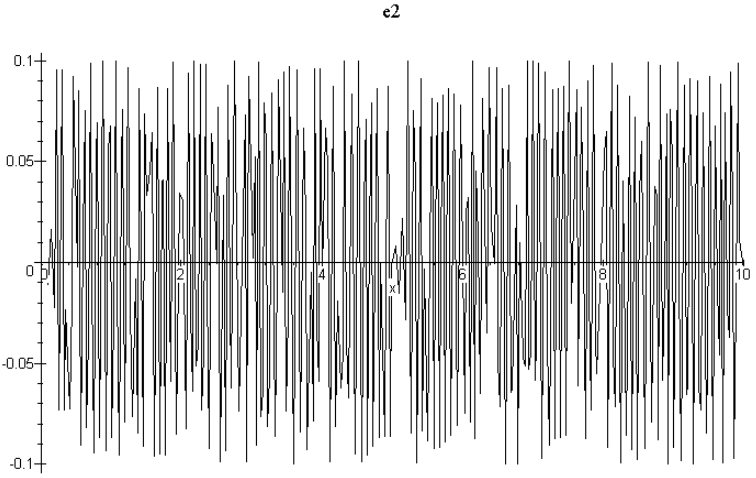

Figure 7.5. Second order wavelet approximation of Young modulus in zeroth scale

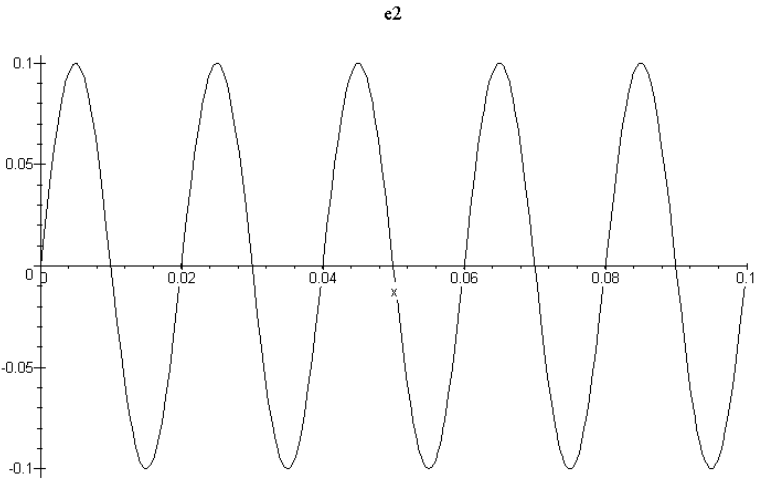

Figure 7.6. Second order wavelet approximation of Young modulus in first scale

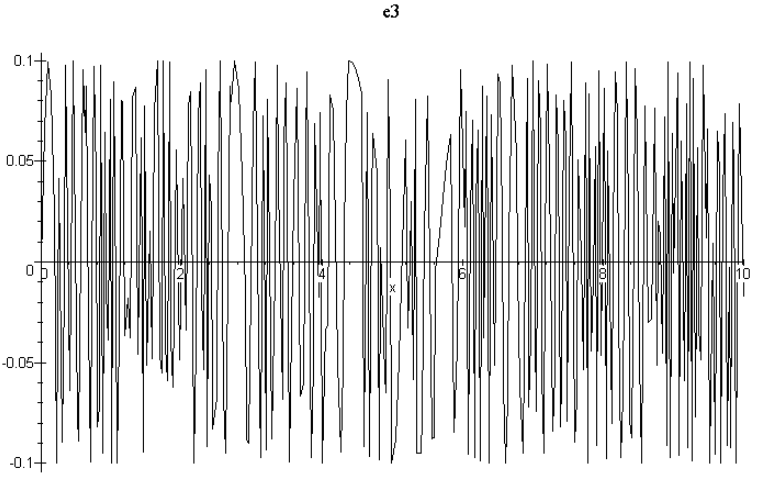

Figure 7.7. Third order wavelet approximation of Young modulus in first scale

As is shown in the next figures (Figures 7.8 and 7.9), using some special combinations of the basic wavelets (Haar, Mexican hat, Gabor, Morlet, Daubechies and/or sinusoidal waves [323]), the spatial variability of Young modulus for the two component composite with and without some interphase can be computationally simulated using a theoretical description of the spatial distribution of this modulus and the symbolic computation package MAPLE, for instance. For illustration of the problem we consider the Representative Volume Element (RVE) of a two−component composite with the following elastic characteristics: e_1=209E9 and e_2=209E8 with the RVE length l=1.0 and equal volume fractions of

both components. The following wavelet function is proposed to achieve the multiscale character of Young modulus spatial variability in the RVE without the interface defects (Figure 7.8):

$$e(x) = h(x) + 0.2\times10^{10}\sin\left(5\times10^{1}x\right) + 0.2\times10^{10}\sin\left(5\times10^{4}x\right)$$

for $h(x)$ being the Haar wavelet function. It can be noticed that, thanks to the multiscale character of the choosen functions, the picture of composite Young modulus shows the randomness on its microscale. However the character of the spatial variability of this modulus is still deterministic. Furthermore, we can illustrate much more complicated and sometimes more realistic effects in composites – the RVE can be almost damaged at the interface and, according to ageing and fatigue processes, the spatial distribution of elastic properties can be far from constant along the heterogeneity main axis. It is approximated by a combination of Haar, some sinusoidal and the so−called Mexican hat wavelets as

$$e(x) = h(x) + 0.2\times10^{10}\sin\left(5\times10^{1}x\right) + 0.2\times10^{10}\sin\left(5\times10^{4}x\right) + 0.6\times10^{10}$$
$$-0.76597\times10^{11}\times\exp\left(-8.00\times x^{2}\right)\times\left(16.0\times x^{2}-1\right)$$

The algebraic structure of this wavelet is a little complicated: however (1) it illustrates very well the capabilities of the wavelet−based approximation of mechanical and physical properties of the real composites, (2) it can be used together with structural image analysis tools for the relevant analyses of composites and (3) it enables direct symbolic homogenisation of such media.

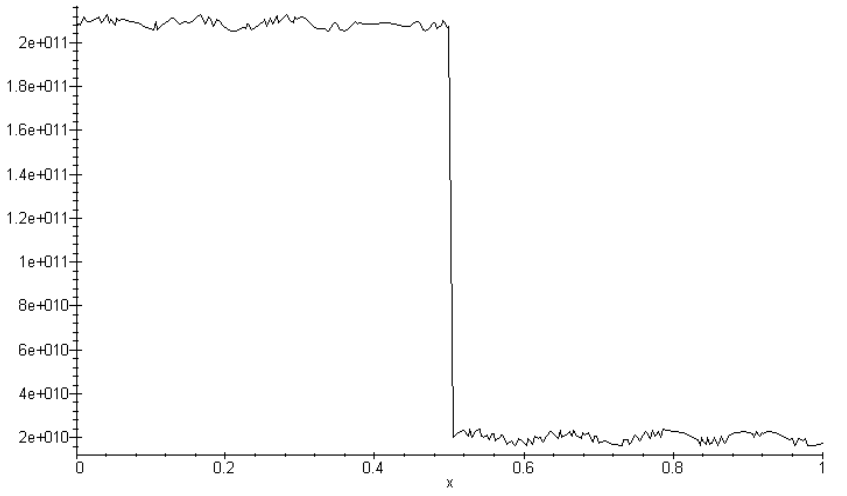

Figure 7.8. Wavelet approximation of elastic properties of two−component composite

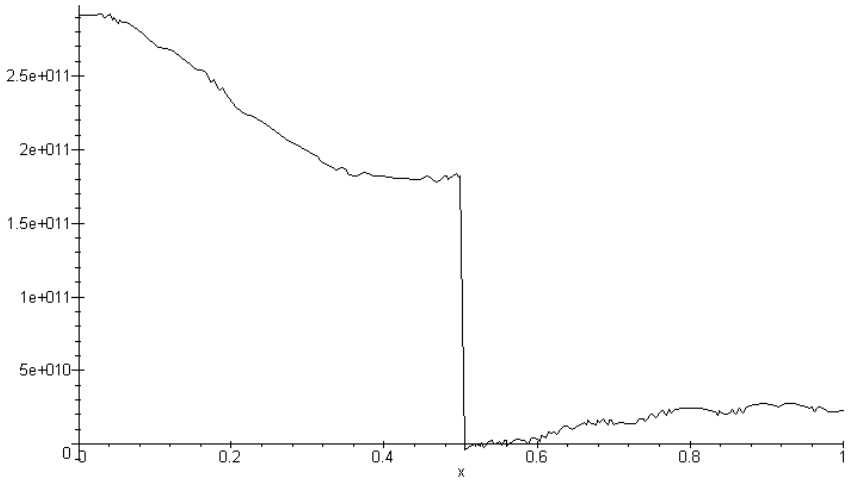

Figure 7.9. Wavelet approximation of the elastic properties of two−component composite with interface defects

As far as this composite is unidirectional, some classical homogenisation closed−form equations can be used to construct the equivalent medium using the relevant differential equilibrium equations directly. In this case it does not matter whether deterministic or probabilistic distribution of material coefficients are given – the PDF symbolic integration can be carried out using a computer. Fortunately, the structural sensitivity analysis may be performed with respect to the variabilities of material properties in quite different scales of the composite; it can be carried out analogously to the considerations presented in [167].

The situation complicates significantly in the case of planar distribution of material tensors, where the cell problems are to be solved by wavelet decomposition and construction to determine the effective behaviour of the entire composite. However, it is mathematically proved in this chapter, that when the structure is heterogeneous in many scales, the effective elastic modulus differs from that obtained for the corresponding classical two−scale and two−component composite beam.

Another disadvantage of the wavelet−based analysis of composite materials is the assumption of a very arbitrary character that the physical model and the accompanying equations of thermodynamical equilibrium have exactly the same form in each scale of the considered medium which follows purely mathematical nature of the wavelet transform. It eliminates the opportunity of the physical transition from the particle scale through chemical interface reactions in various composites to the global scale of the entire engineering structure. It reflects the intuitive feeling that the transition between the corresponding medium scale must strongly depend on the physical scale we are operating on.

7.2 Multiscale Reduction and Homogenisation

Therefore, a multiresolutional homogenisation method is proposed for numerical analysis together with various stochastic computational techniques, which makes it possible to determine probabilistic characteristics of various multiscale composites. Considering the fact that the multiresolutional method makes it possible to determine the effective physical characteristics in a closed form, the stochastic second order perturbation approach is applied to analyse the multiscale randomness of the entire composite in the most general form.

Let us consider the following differential equilibrium equation to distinguish the differences between a classical asymptotic approach and multiresolutional scheme:

$$-\frac{d}{dx}\left(e(x)\frac{d}{dx}u(x)\right)=f(x);\qquad x\in[0,1] \tag{7.1}$$

where $e(x)$, defining material properties of the heterogeneous medium, varies arbitrarily on many scales (macro, meso and micro, etc.). The unit interval denotes here the Representative Volume Element (RVE), also called the periodicity cell.

The classical result obtained through the asymptotic homogenisation theory is given by (2.71) for deterministic composites exhibiting two separate geometrical scales linked by the scale parameter ε – this is the weakest point of this approach. Sometimes ε is treated as a positive real number tending to 0 (practically an infinite number of the RVEs in the composite) and, alternatively, some small positive parameter. As it can be demonstrated, the essential differences are observed in these two models. Now, this parameter is treated as some real functions introduced as the wavelet function relating two or more separate geometrical scales of the composite.

In contrast to the classical approach to the homogenisation problem, the multiresolution approach uses the algebraic transformation between scales provided by the multiresolution analysis to solve for the fine−scale behaviour and explicitly eliminate it from the equation. This approach has the advantage that the coefficients may vary on arbitrarily many scales. The chain of subspaces

$$\ldots\subset V_2\subset V_1\subset V_0\subset V_{-1}\subset V_{-2}\subset\ldots \tag{7.2}$$

defines the hierarchy of scales that the multiresolution scheme uses. This chain of subspaces is defined in such a way that the space V_j is "finer" than the space V_{j+1} in the sense that (1) all of V_{j+1} is contained in V_j, and (2) the component of V_j which is not in V_{j+1} consists of functions which resolve features on a scale finer than any function in V_{j+1} may resolve. The difference between successive spaces in this chain is captured by the so−called wavelet space W_{j+1}, defined to the

orthogonal complement of V_{j+1} in V_j. An orthogonal basis for the wavelet space W_{j+1} is constructed which has vanishing moments, i.e. the basis elements are L^2-orthogonal to low−degree polynomials. The existence of orthogonal wavelet bases with vanishing moments distinguishes the multiresolution approach from typical multi−scale discretisations provided by finite−element or hierarchical bases. If we are considering a multiresolution analysis defined on a bounded domain, then the hierarchy of scales defined above has the coarsest scale (which is called V_0), and we write instead

$$V_0 \subset V_{-1} \subset V_{-2} \subset \ldots \tag{7.3}$$

Let us review the multiresolution strategy for the reduction and homogenisation of linear problems. Let us consider to this purpose a bounded linear operator $S_j : V_j \to V_j$. Since V_j is spanned by translations of the function $\phi\left(2^j x - k\right)$, we know that the operator S_j may be written in the form of a matrix. If the multiresolution analysis is defined on a bounded domain, then this matrix is finite; otherwise it is an infinite matrix, which we consider as an operator on L^2. Let us consider the equation

$$S_j x = f \tag{7.4}$$

The decomposition $V_j = V_{j+1} \oplus W_{j+1}$ allows us to split the operator S_j into four pieces (recall that W_{j+1} is called the wavelet space and is the "detail" or fine−scale component of V_j) and write

$$\begin{pmatrix} A_{S_j} & B_{S_j} \\ C_{S_j} & T_{S_j} \end{pmatrix} \begin{pmatrix} d_x \\ s_x \end{pmatrix} = \begin{pmatrix} d_f \\ s_f \end{pmatrix} \tag{7.5}$$

where we have

$$\begin{aligned} A_{S_j} &: W_{j+1} \to W_{j+1} \\ B_{S_j} &: V_{j+1} \to W_{j+1} \\ C_{S_j} &: W_{j+1} \to V_{j+1} \\ T_{S_j} &: V_{j+1} \to V_{j+1} \end{aligned} \tag{7.6}$$

and $d_x, d_y \in W_{j+1}$, $s_x, s_y \in V_{j+1}$ are the L^2-orthogonal projections of x and f onto the W_{j+1} and V_{j+1} spaces. The projection s_x is thus the coarse−scale component of

the solution x and d_x is its fine−scale component. Formally eliminating d_x from (7.5) by substituting $d_x = A_{S_j}^{-1}\left(d_f - B_{S_j} s_x\right)$ yields

$$\left(T_{S_j} - C_{S_j} A_{S_j}^{-1} B_{S_j}\right) s_x = s_f - C_{S_j} A_{S_j}^{-1} d_f \tag{7.7}$$

This equation is called a reduced equation, while the operator

$$R_{S_j} = T_{S_j} - C_{S_j} A_{S_j}^{-1} B_{S_j} \tag{7.8}$$

is a one step reduction of the operator S_j also known as the Schur complement of the block matrix $\begin{pmatrix} A_{S_j} & B_{S_j} \\ C_{S_j} & T_{S_j} \end{pmatrix}$.

Note that the solution s_x of the reduced equation is exactly $P_{j+1}x$, where P_{j+1} is the projection onto V_{j+1} and x is the solution of (7.4). Note that the reduced equation is not the same as the averaged equation, which is given by

$$T_{S_j} \tilde{s}_x = s_f \tag{7.9}$$

Once we have obtained the reduced equation, it may formally be reduced again to produce an equation on V_{j+2} and the solution of this equation is just the V_{j+2} component of the solution for (7.4). Likewise, we may reduce these equations recursively n times (assuming that, if the multiresolution analysis is on a bounded domain, then $j+n \le 0$) to produce an equation on V_{j+n}, the solution of which is the projection of the solution of (7.4) on V_{j+n}.

We note that in the finite−dimensional case, if we are considering a multiresolution analysis defined on a domain in $\mathbf{R}$, the reduced equation (7.5) has half as many unknowns as the original equation (7.4). If the domain is in $\mathbf{R}^2$, then the reduced equations have one−fourth as many unknowns as the original equation. Reduction, therefore, preserves the coarse−scale behaviour of solutions while reducing the number of unknowns.

In order to iterate the reduction step over many scales, we need to preserve the form of the equation as a way of deriving a recurrence relation. In (7.4) and (7.5), both S_j and R_{S_j} are matrices, and thus the procedure may be repeated. However, identification of the matrix structure is usually not sufficient. In particular, even though the matrix $\mathbf{A}$ for ODEs and PDEs is sparse, the component $A_{S_j}^{-1}$ term may become dense, changing the equation from a local one to a global one. It is important to know under what circumstances the local nature of the differential

operator may be (approximately) preserved. Furthermore, if the equation is of the form of

$$-\nabla\big(e(x)\nabla u(x)\big)= f(x) \tag{7.10}$$

or some other variable–coefficient differential equation, we should verify if the reduction procedure preserves this form, so that we may find effective coefficients of the equation on the coarse scale. This process is the basic goal of homogenisation techniques, and it extracts information from the reduced equation based on the form of the original equation. Thus, within the multiresolution approach, reduction and homogenisation are closely related but have different goals: homogenisation attempts to find effective equations and their coefficients on the coarse scale, whereas reduction merely finds a coarse–scale version of a given system of equations.

The multiresolutional (MRA) homogenisation procedure is applied to the systems of ODEs, which may be written in the form

$$Bx + q + \lambda = K\big(Ax + p\big) \tag{7.11}$$

In particular, we consider equations of the form

$$\big(I + B(t)\big)x(t) + q(t) + \lambda = \int_0^t \big(A(s)x(s) + p(s)\big)\,ds\ ,\ t \in (0,1) \tag{7.12}$$

on $L^2(0,1)$, where $B(t)$ and $A(t)$ are n x n matrix–valued functions, $p(t)$ and $q(t)$ are vector forcing terms, and $x(t)$ is the solution vector. As a differential equation this is written as

$$\frac{d}{dt}\Big(\big(I + B(t)\big)x(t) + q(t)\Big)= A(t)x(t) + p(t) \tag{7.13}$$

with the initial conditions $\big(I + B(0)\big)x(0) = -q(0) - \lambda$. On V_j, j<0, the projection of (7.11) is written as

$$B_j x_j + q_j + \lambda = K_j\big(A_j x_j + p_j\big) \tag{7.14}$$

or

$$S_j x_j = f_j \tag{7.15}$$

where

$$S_j = B_j - K_j A_j\ ,\ f_j = K_j p_j - q_j - \lambda\ ,\ x_j = P_j x_j \tag{7.16}$$

After a single reduction, our goal is to have an equation on V_{j+1} of the form

$$B_{j+1}^{(j)} x_{j+1}^{(j)} + q_{j+1}^{(j)} + \lambda = K_{j+1}\left(A_{j+1}^{(j)} x_{j+1}^{(j)} + p_{j+1}^{(j)}\right) \tag{7.17}$$

where $x_{j+1}^{(j)} = P_{j+1} x_j$, $B_{j+1}^{(j)} = P_{j+1} x_j$, etc. We use the notation $B_l^{(j)}$ to indicate that the equation is first projected to a scale V_j, and then the reduction procedure is applied *l-j* times to obtain an equation on V_l. This notation therefore indicates that (7.17) was obtained by a single reduction of the same form of equation on V_j one time to produce an equation on the coarser scale V_{j+1}.

It allows one to establish a recurrence relation for $k=j,j+1,...,0$ between the operators and forcing terms $B_k^{(j)}, x_k^{(j)}, p_k^{(j)}, q_k^{(j)}$ on V_{k+1}. It turns out that this task of finding the recurrence relations is simplified significantly if one uses a multiresolution analysis whose basis functions have non−overlapping support. We use the Haar basis, but a multiwavelet basis may be used if higher order elements are necessary.

In the Haar basis, the operators B_j, A_j and K_j derived from equations of the form of (7.14) have a simple form. Each of these is in an ($N_j n$) x ($N_j n$) matrix, where $N_j=2^j$ is the number of unknowns on the scale V_j and n denotes the number of equations in the original system. Furthermore, B_j and A_j are both block-diagonal matrices. The diagonal blocks of B_j and A_j are n x n matrices. There are therefore N_j diagonal blocks, each of which is an n x n matrix. For B_j and A_j we denote their ith diagonal blocks by $\left(B_j\right)_i$ and $\left(A_j\right)_i$. The matrices are given by the Haar coefficients of the n x n matrix−valued functions $B(x)$ and $A(x)$ on the scale V_j. It can be written that

$$B_j = diag\left\{I + \left(B_j\right)_i\right\}_{i=0}^{i=2^j-1} \tag{7.18}$$

and

$$A_j = diag\left\{\left(A_j\right)_i\right\}_{i=0}^{i=2^j-1} \tag{7.19}$$

where

$$K_j = \delta_j \begin{pmatrix} \frac{1}{2}I & 0 & 0 & \dots & 0 \\ I & \frac{1}{2}I & 0 & \dots & 0 \\ I & I & \frac{1}{2}I & & \dots \\ \dots & & & \dots & \\ I & \dots & & I & \frac{1}{2}I \end{pmatrix} \tag{7.20}$$

where $\delta_j = 2^{-j}$, I is the n x n identity matrix, and $\left(B_j\right)_i$ and $\left(A_j\right)_i$ are the ith Haar coefficients on scale V_j of the n x n matrix−value functions $B(x)$ as well as $A(x)$. For (7.17), the recursion relations are given by

$$\left(A_{k+1}^{(j)}\right)_i = \left(S_A\right)_i - \left(D_A\right)_i F^{-1}\left(\left(D_B\right)_i + \frac{\delta_k}{2}\left(S_A\right)_i\right) \tag{7.21}$$

$$\left(B_{k+1}^{(j)}\right)_i = \left(S_B\right)_i - \frac{\delta_k}{2}\left(D_A\right)_i - \left(\left(D_B\right)_i - \frac{\delta_k}{2}\left(S_A\right)_i\right)F^{-1}\left(\left(D_B\right)_i + \frac{\delta_k}{2}\left(S_A\right)_i\right) \tag{7.22}$$

$$\left(p_{k+1}^{(j)}\right)_i = \left(S_p\right)_i - \frac{\delta_k}{2}\left(D_A\right)_i F^{-1}\left(\left(D_q\right)_i + \left(S_p\right)_i\right) \tag{7.23}$$

$$\left(q_{k+1}^{(j)}\right)_i = \left(S_q\right)_i - \frac{\delta_k}{2}\left(D_p\right)_i - \frac{\delta_k}{2}\left(\left(D_B\right)_i - \left(S_A\right)_i\right)F^{-1}\left(\left(D_q\right)_i - \left(S_p\right)_i\right) \tag{7.24}$$

where

$$\left(S_A\right)_i = \tfrac{1}{2}\left(\left(A_k^{(j)}\right)_{2i} + \left(A_k^{(j)}\right)_{2i+1}\right), \quad \left(D_A\right)_i = \tfrac{1}{2}\left(\left(A_k^{(j)}\right)_{2i} - \left(A_k^{(j)}\right)_{2i+1}\right) \tag{7.25}$$

$$\left(S_B\right)_i = \tfrac{1}{2}\left(\left(B_k^{(j)}\right)_{2i} + \left(B_k^{(j)}\right)_{2i+1}\right), \quad \left(D_B\right)_i = \tfrac{1}{2}\left(\left(B_k^{(j)}\right)_{2i} - \left(B_k^{(j)}\right)_{2i+1}\right) \tag{7.26}$$

$$\left(S_p\right)_i = \tfrac{1}{\sqrt{2}}\left(\left(p_k^{(j)}\right)_{2i} + \left(p_k^{(j)}\right)_{2i+1}\right), \quad \left(D_p\right)_i = \tfrac{1}{\sqrt{2}}\left(\left(p_k^{(j)}\right)_{2i} - \left(p_k^{(j)}\right)_{2i+1}\right) \tag{7.27}$$

$$\left(S_q\right)_i = \tfrac{1}{\sqrt{2}}\left(\left(q_k^{(j)}\right)_{2i} + \left(q_k^{(j)}\right)_{2i+1}\right), \quad \left(D_q\right)_i = \tfrac{1}{\sqrt{2}}\left(\left(q_k^{(j)}\right)_{2i} - \left(q_k^{(j)}\right)_{2i+1}\right) \tag{7.28}$$

and, finally,

$$F = I + \left(S_B\right)_i + \frac{\delta_k}{2}\left(D_A\right)_i \tag{7.29}$$

Note that the recurrence relations are local and can be carried out over many scales as needed (assuming the existence of F^{-1} at each scale). Starting with (7.17) on V_{-j} and, reducing j times, yields on V_0

$$B_0^{(j)} x_0^{(j)} + q_0^{(j)} + \lambda = K_0\left(A_0^{(j)} x_0^{(j)} + p_0^{(j)}\right) \tag{7.30}$$

where to compute $B_0^{(j)}, A_0^{(j)}, p_0^{(j)}, q_0^{(j)}$ we use the recurrence relations j times.

Multiresolutional homogenisation is formulated as follows. First, we consider the limit of (7.30) as $j \to -\infty$, therefore

$$B_0^{(-\infty)} x_0^{(-\infty)} + q_0^{(-\infty)} + \lambda = K_0 \left(A_0^{(-\infty)} x_0^{(-\infty)} + p_0^{(-\infty)} \right) \tag{7.31}$$

It is employed to eliminate infinite number of fine scales from the original equation. The matrices $B_0^{(-\infty)}, A_0^{(-\infty)}$ are called the reduced coefficients of (7.14). Then, we look for the operators and forcing terms $B^h(t), A^h(t), p^h(t), q^h(t)$ with certain desired qualities (e.g. constant values) such that the equation

$$\left(I + B^h(t) \right) x(t) + q^h(t) + \lambda = \int_0^t \left(A^h(s) x(s) + p^h(s) \right) ds \,, \quad t \in (0,1) \tag{7.32}$$

subjected to the same reduction and limit procedure as (7.12), yields on V_0 the same equation as in (7.31). For (7.12) we usually require that B^h, A^h, p^h, q^h be constant. The result of homogenisation in this case is summarised as follows:

Theorem

Given (7.12), if the limits, which determine the matrices $B_0^{(-\infty)}$ and $A_0^{(-\infty)}$ exist, then there exist constant matrices B^h, A^h and forcing terms p^h, q^h, such that the reduced coefficients and forcing terms of (7.32) are given by $B_0^{(-\infty)}, A_0^{(-\infty)}, q_0^{(-\infty)}, p_0^{(-\infty)}$. The homogenised coefficients B^h, A^h and forcing terms p^h, q^h are defined by

$$A^h = A_0^{(-\infty)} \tag{7.33}$$

$$B^h = A^h \tilde{A}^{-1} - I \tag{7.34}$$

$$p^h = p_0^{(-\infty)} \tag{7.35}$$

$$q^h = q_0^{(-\infty)} + \left(I - \tfrac{1}{2} \tilde{A} - \tilde{A} \left(\exp\left(\tilde{A} - I \right)^{-1} A^h \right)^{-1} p^h \right) \tag{7.36}$$

where

$$\tilde{A} = \log\left(I + \left(I + B_0^{(-\infty)} - \tfrac{1}{2} A^h \right)^{-1} A^h \right) \tag{7.37}$$

Proof

It is observed that for the constant coefficients the recurrence relations (7.21) and (7.22) simplify to

$$A_{k+1}^h = A_k^h \tag{7.38}$$

$$B_{k+1}^h = B_k^h + \frac{\delta_k^2}{4} A_k^h \left(I + B_k^h\right)^{-1} A_k^h \tag{7.39}$$

Likewise, the recurrence relations for the forcing terms simplify to

$$p_{k+1}^h = p_k^h \tag{7.40}$$

$$q_{k+1}^h = q_k^h - \frac{\delta_k}{2} A_k^h \left(I + B_k^h\right)^{-1} p_k^h \tag{7.41}$$

Since the term A^h is unchanged by reduction, it is clear that $A^h = A_0^{(-\infty)}$. Similarly, p^h is unchanged by reduction, so $p^h = p_0^{(-\infty)}$. The situation for B^h and q^h is more complicated. We solve for them analytically using the solution of (7.32). Consider the case $p_0^{(-\infty)} = 0$. Clearly, then, it is the case that $q^h = q_0^{(-\infty)}$. The solution of (7.32) is therefore given by

$$x(t) = -\exp\left(\tilde{A}t\right)\tilde{q} \tag{7.42}$$

where $\tilde{A} = \left(I + B^h\right)^{-1} A^h$, $\tilde{q} = \left(I + B^h\right)^{-1}\left(q^h + \lambda\right)$. The average of this solution must also solve (7.31) since it is the equation for the average value of the solution by definition. The average value of $x(t)$ in (7.32) on the interval [0,1] is given by

$$\langle x \rangle = \left(-\int_0^1 \exp\left(\tilde{A}t\right) dt \right) \tilde{q} = \left(I - \exp\left(\tilde{A}\right)\right) \tilde{A}^{-1} \tilde{q} \tag{7.43}$$

The solution to (7.31) is given by

$$x_0^{(-\infty)} = -\left(I + B_0^{(-\infty)} - \tfrac{1}{2} A_0^{(-\infty)}\right)^{-1} \left(q_0^{(-\infty)} + \lambda\right) \tag{7.44}$$

The right hand sides of (7.43) and (7.44) are demonstrated to be equal for all λ; setting λ=0 and solving for B^h yields the solution given in the statement of the proposition. The case when $p_0^{(-\infty)} \neq 0$ proceeds similarly.

Solutions of (7.32) have the same "average" or coarse−scale behaviour as solutions of (7.12). The main point is that this homogenisation procedure allows for coefficients to vary on arbitrarily many intermediate scales, which is in contrast to the classical homogenisation examples, which did not allow for intermediate scales.

As formulated above, the multiresolution approach to homogenisation requires the computation of $A_0^{(-\infty)}$ and $B_0^{(-\infty)}$, i.e. a limit over infinitely many scales. The typical practice is to compute successive $A_0^{(-J)}$ and $B_0^{(-J)}$ terms until finer approximations vary by less than some specified tolerance, and use these matrices as approximations to $A_0^{(-\infty)}$ and $B_0^{(-\infty)}$.

Besides establishing the general framework for multiresolution reduction and homogenisation, it is observed that for systems of linear ordinary differential equations, using the Haar basis (or a multiwavelet basis) provides a technical advantage. Since the functions of the Haar basis on a fixed scale do not have overlapping supports, the recurrence relations for the operators and forcing terms in the equation may be written as local relations and solved explicitly. Thus, for ODEs, an explicit local reduction and homogenisation procedure is possible.

Let us consider for illustration (7.1) with initial conditions at x=0. It may be rewritten as the coupled first−order system

$$\begin{cases} \dfrac{d}{dx} v(x) = -f(x) \\ \dfrac{d}{dx} u(x) = e(x)^{-1} v(x) \end{cases} \tag{7.45}$$

By writing in an integral form one can obtain

$$\begin{pmatrix} u(x) \\ v(x) \end{pmatrix} - \begin{pmatrix} u(0) \\ v(0) \end{pmatrix} = \int_0^x \left(\begin{pmatrix} 0 & e(t)^{-1} \\ 0 & 0 \end{pmatrix} \begin{pmatrix} u(t) \\ v(t) \end{pmatrix} + \begin{pmatrix} 0 \\ -f(t) \end{pmatrix} \right) dt \tag{7.46}$$

Thus, in the notation of (7.11), $B(x)$=0, $A(x) = \begin{pmatrix} 0 & e(x)^{-1} \\ 0 & 0 \end{pmatrix}$, $\lambda = \begin{pmatrix} u(0) \\ v(0) \end{pmatrix}$ and $q(t)$=0 as well as $p(t) = \begin{pmatrix} 0 \\ -f(t) \end{pmatrix}$.

Using the reduction procedure in the Haar basis for a system of linear differential equations, the goal is to find constants B^h, A^h, p^h, q^h such that

$$\left(I + B^h\right) \begin{pmatrix} u(x) \\ v(x) \end{pmatrix} + q^h + \lambda = \int_0^x \left(A^h \begin{pmatrix} u(t) \\ v(t) \end{pmatrix} + p^h \right) dt \tag{7.47}$$

after reduction to the scale V_0 will be the same as (7.46) reduced to that scale. This is accomplished by solving the recursion relations between the operators in the reduced equations explicitly, element−by−element in each matrix. This is possible to do because of the non−overlapping supports of the Haar basis functions on a fixed scale. The result for the first two coefficients is

$$B^h = \begin{pmatrix} 0 & 0 \\ 0 & 0 \end{pmatrix}, A^h = \begin{pmatrix} 0 & M_1 - 2M_2 \\ 0 & 0 \end{pmatrix} \tag{7.48}$$

where

$$M_1 = \int_0^1 \frac{1}{e(t)}\,dt\,,\ M_2 = \int_0^1 \frac{t-\frac{1}{2}}{e(t)}\,dt \tag{7.49}$$

Similar expressions for p^h and q^h can be found. Note that we have $p^h = q^h = 0$ if $f(x)$=0 identically. Furthermore, in general B^h, A^h do not depend on p and q. As a first−order system of ordinary differential equations, the homogenised equation yields

$$\begin{cases} \dfrac{d}{dx} v(x) = f^h(x) \\ \dfrac{d}{dx} u(x) = (M_1 - 2M_2)\, v(x) \end{cases} \tag{7.50}$$

what is somewhat different from the classical result. This difference results from the fact that the multiresolution homogenisation procedure allows the coefficients $e(x)$ to vary on arbitrarily many scales, whereas the classical approach presented before allows only for coefficients of the form $e(x/\varepsilon)$. In the multiresolution context this amounts to restricting the coefficients to an asymptotically fine scale. Let us apply the same limit in the preceding section to the coefficients appearing in the multiresolution approach. We start with the coefficients of the form $e(x/\varepsilon)$.

Applying this homogenisation scheme to the elliptic equation with these coefficients yields two terms, $M_1(\varepsilon)$ and $M_2(\varepsilon)$. If we take the limit as $\varepsilon \to 0$, it is found that

$$\lim_{\varepsilon \to 0} M_1(\varepsilon) = M_1 \tag{7.51}$$

and

$$\lim_{\varepsilon \to 0} M_2(\varepsilon) = 0 \tag{7.52}$$

Thus, the factor M_2 is present in the multiresolution context but does not appear in the classical approach, and it is zero when the limit found in the classical method is applied to the result of the multiresolution methodology.

Let us note that this formula of the homogenised parameter $e^{(eff)}$ introduces new, closer bounds on the wavelet function defining material parameters than is done by classical formulation: integrals $\int_0^L \frac{dx}{e(x)}$ and $\int_0^L \frac{xdx}{e(x)}$ must be of real values and $e(x)$ must be positive defined to assure homogenisability of the problem. The counter−example is the family of sinusoidal wavelets of the form $e(x) = e_0 + \alpha \sin\left(\frac{\pi x}{L}\right)$, where $e_0, \alpha, L \in \Re$. Taking for example L=10, e_0=20 and α=0.1, MAPLE symbolic integration returns $\int_0^L \frac{xdx}{e(x)} = -2.99242 - 19.07199i$. The classical small parameter homogenisation method should be applied in that case; otherwise another wavelet decomposition of the real composite is to be performed.

7.3 Multiscale Homogenisation for the Wave Propagation Equation

For illustration, let us consider the following ordinary differential equation (ODE) corresponding to unidirectional acoustic wave propagation in a multiscale medium with uniaxial distribution of nonhomogeneities [71,188]:

$$\frac{d}{dx}u(x) = i\omega M(x)u(x); \quad x \in [0,1] \tag{7.53}$$

where physical coefficients $M(x)$ for both composite layers are defined by

$$M(x) = \begin{cases} M_0, 0 \le x < \frac{1}{2} \\ M_1, \frac{1}{2} \le x \le 1 \end{cases} \tag{7.54}$$

These equations are solved using the methods typical for a deterministic problem and are derived for equal volume ratios of both layers. Otherwise, they should be complemented with the ratios c_1 and c_2. The corresponding homogenised equation can be rewritten for the deterministic system as

$$\frac{d}{dx}u(x) = K^{(eff)}u(x) \tag{7.55}$$

It can be demonstrated [71] that the homogenised coefficient $K^{(eff)}$ is equal to

$$K^{(eff)} = \log\left(I + \left(I + B_0^{(-\infty)} - \tfrac{1}{2}A_0^{(-\infty)}\right)^{-1} A_0^{(-\infty)}\right) \tag{7.56}$$

for

$$B_0^{(-\infty)} = S'_B - \tfrac{1}{4} D'_A - \left(D'_B - \tfrac{1}{4} S'_A\right) F^{-1} \left(D'_B + \tfrac{1}{4} S'_A\right) \tag{7.57}$$

and

$$A_0^{(-\infty)} = S'_A - D'_A F^{-1} \left(D'_B + \tfrac{1}{4} S'_A\right) \tag{7.58}$$

The right hand side coefficients denote

$$S'_A = \tfrac{1}{2}\left(\left(A_1^{(-\infty)}\right)_0 + \left(A_1^{(-\infty)}\right)_1\right), \quad D'_A = \tfrac{1}{2}\left(\left(A_1^{(-\infty)}\right)_0 - \left(A_1^{(-\infty)}\right)_1\right) \tag{7.59}$$

$$S'_B = \tfrac{1}{2}\left(\left(B_1^{(-\infty)}\right)_0 + \left(B_1^{(-\infty)}\right)_1\right), \quad D'_B = \tfrac{1}{2}\left(\left(B_1^{(-\infty)}\right)_0 - \left(B_1^{(-\infty)}\right)_1\right) \tag{7.60}$$

$$F = I + S'_B + \tfrac{1}{4} D'_A \tag{7.61}$$

where

$$A_j^{(-\infty)} = \lim_{J\to\infty} A_j^{(1-J)}, \quad B_j^{(-\infty)} = \lim_{J\to\infty} B_j^{(1-J)} \tag{7.62}$$

After some algebra it is found that

$$\left(A_1^{(-\infty)}\right)_j = A_j, \quad \left(B_1^{(-\infty)}\right)_j = \frac{A_j}{2}\left(\left(\exp\left(\frac{A_j}{2}\right) - I\right)^{-1} + \frac{1}{2} I\right) - I, \quad j=1,2 \tag{7.63}$$

where the following extension is used:

$$\begin{aligned} exp\left(\frac{A_j}{2}\right) &= exp\left(\frac{i\omega}{2} M_j\right) \\ &= I + \frac{i\omega}{2} M_j - \frac{\omega^2}{8} M_j^2 + \frac{i\omega^3}{48} M_j^3 + \ldots + O(\omega^n) \end{aligned} \tag{7.64}$$

Taking into account that the coefficients B and A in (7.63) represent physical properties of the composite components with the total number of various scales tending to infinity, it is possible to determine an analogous definition of the homogenised coefficient for a composite with some finite scale number. Furthermore, using the stochastic second order perturbation second probabilistic moment methodology, it is relatively easy to determine the first two probabilistic moments of the homogenised coefficient defined by (7.63).

Further, real and imaginary parts of $K^{(eff)}$ are computed according to (7.56)−(7.58). The following data are adopted: M_0=10.0, M_1=1.0 with c_1=c_2=0.5, where the parameter $\omega \to 0$ (cf. Figures 7.10 and 7.11) and $\omega \to \infty$ (see Figs. 7.12 and 7.13). As can be observed, the real and imaginary parts tend to 0 in both cases, which finally gives $K^{(eff)} \to 0$, too. Further, such a combination of input parameters results in a minimum of the $K^{(eff)}$ real part for $\omega \approx 1.15$. On the other hand, the singularity of $\mathrm{Im}(K^{(eff)})$ is obtained with $\omega \approx 0.75$.

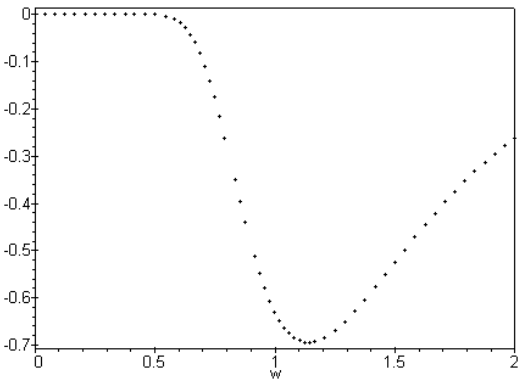

Figure 7.10. Real part of $K^{(eff)}$ near 0

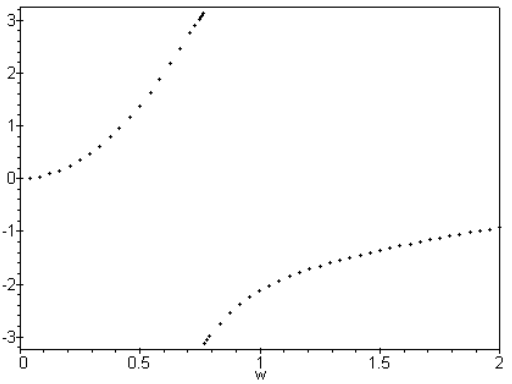

Figure 7.11. Imaginary part of $K^{(eff)}$ near 0

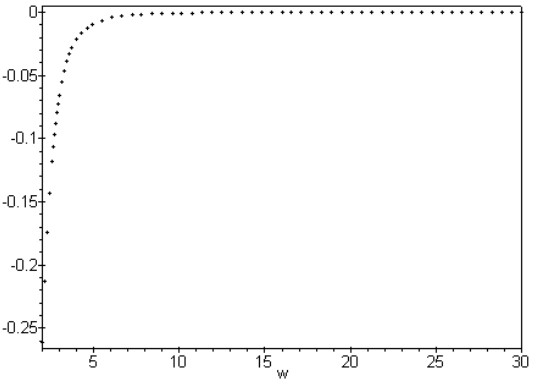

Figure 7.12. Real part of $K^{(eff)}$ in ω domain

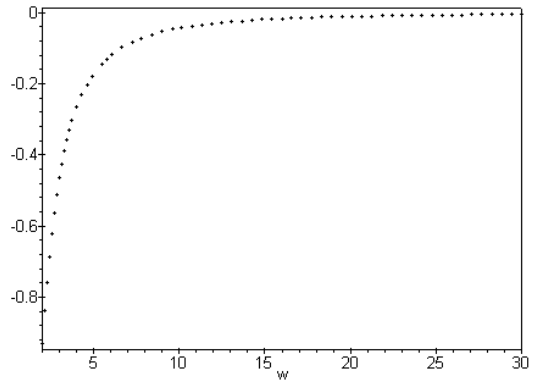

Figure 7.13. Imaginary part of $K^{(eff)}$ in ω domain

Next, the effective parameter in its real and imaginary part is determined as a function of the ω value and the ratio relating material parameters of the composite components M_0=2−20. The results are presented in Figures 7.14 and 7.15 below. As can be compared with Figures 7.12 and 7.13, the material parameter interrelation influences significantly the effective parameters in the same range as the ω values. Analogous limiting values in real and imaginary parts of the homogenised parameter as well as imaginary part singularities are noticed as second order functions of both design parameters of the study.

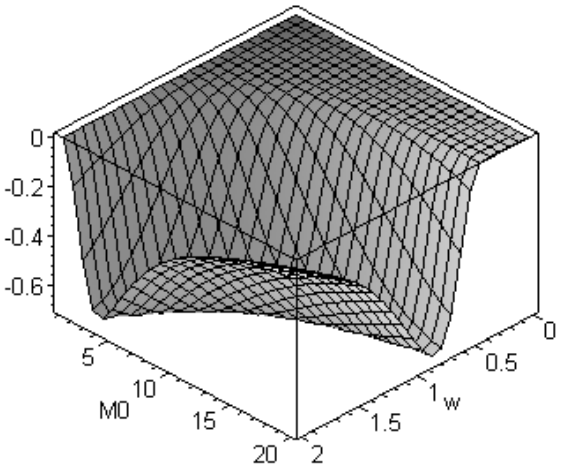

Figure 7.14. Real part of $K^{(eff)}$

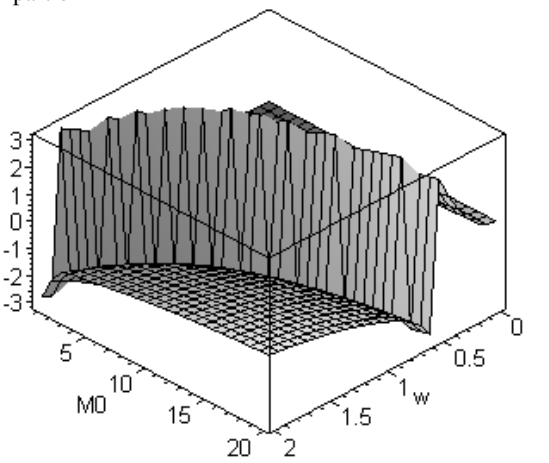

Figure 7.15. Imaginary part of $K^{(eff)}$

Probabilistic moments of real and imaginary surfaces are expected in the probabilistic case. However a more important problem (from the physical point of view) is to determine the relations for homogenised coefficients in terms of volume fractions of the layers as well as to extend the homogenisation method to the heterogeneous multiscale media with a more general periodic geometry of the RVE. The entire methodology can be adopted with minor changes to computational analysis of the wave propagation in random media [26], where material properties are defined using a combination of harmonic functions with random coefficients.

7.4 Introduction to Multiresolutional FEM Implementation

Let us consider the following boundary value problem for a homogeneous medium:

$$-e\nabla^2 u + \gamma u = f\,, \quad x \in \Omega \tag{7.65}$$

with

$$u = 0\,, \quad x \in \Gamma_u \subset \partial\Omega \tag{7.66}$$

The variational formulation of this problem for the multiscale medium for k=1,…,n, indexing its various scales is obtained at the scale k as

$$\int_\Omega e\nabla u_k \nabla \varphi_k d\Omega + \int_\Omega \gamma u_k \varphi_k d\Omega = \int_\Gamma f\varphi_k d\Gamma\,, \quad x \in \Omega \tag{7.67}$$

Solution of the problem must be found recursively by using some transformation between neighbouring medium scales. That is why the following nonsingular n x n wavelet transform matrix W_k is introduced:

$$\mathbf{W}_k = \mathbf{T}_k \begin{bmatrix} \mathbf{T}_{k-1} & 0 \\ 0 & \mathbf{I}_{k-1} \end{bmatrix} \tag{7.68}$$

where I_k is an identity matrix and

$$\boldsymbol{\psi}_k = \mathbf{W}_k^T \boldsymbol{\varphi}_k \tag{7.69}$$

T_k is a two−scale transform such that

$$\begin{Bmatrix} \boldsymbol{\varphi}_{k-1} \\ \boldsymbol{\psi}_k \end{Bmatrix} = \mathbf{T}_k^T \boldsymbol{\varphi}_k \tag{7.70}$$

with

$$\psi_k^j = \varphi_k^{2j-1}\,, \quad \text{j=1,…,N}_\text{k} \tag{7.71}$$

where N_k denotes the total number of the FEM nodal points at the scale k. Let us illustrate the wavelet–based FEM idea using the example of a 1D linear two–node finite element. The classical shape functions are defined as [78]

$$\mathbf{N}^T = \begin{Bmatrix} N_1 \\ N_2 \end{Bmatrix} = \begin{Bmatrix} \frac{1}{2}(1-\xi) \\ \frac{1}{2}(1+\xi) \end{Bmatrix} \tag{7.72}$$

where N_1 is valid for ξ=-1 and N_2 – for ξ=1. The scale effect is introduced on the finite element level by inserting new extra degrees of freedom at each new scale. Then, the scale 1 corresponds to one multiscale DOF per the original finite element, scale 2 to two multiscale DOFs, etc., which may be characterised as [66]

$$\psi_k(\xi) = \psi_k\left(2^{k-1}(1+\xi) - 2j - 1\right) \tag{7.73}$$

and

$$\begin{cases} 2^{2-k} j - 1 \le \xi \le 2^{2-k} j + 2^{1-k} - 1 \\ 2^{2-k} j + 2^{1-k} - 1 \le \xi \le 2^{2-k} j + 2^{2-k} - 1 \end{cases} \tag{7.74}$$

where k defines the actual scale, while j characterises the translates in the finite element parametric space. Thus, the reconstruction algorithm starts from the original solution for the original mesh and next, introduction of the new scales is made using the reconstruction

$$\mathbf{u}_k^{2+2^{k-1}+j} = \sum_{i=1}^{N_{old}} \mathbf{N}_i \mathbf{u}_0^i + \sum_{i=1}^{N_{new}} \boldsymbol{\psi}_k^{2+2^{k-1}+j} \Delta \mathbf{u}_k^{2+2^{k-1}+j} \tag{7.75}$$

The wavelet algorithm for stiffness matrix reconstruction starts at scale 0 with the stiffness matrix

$$\mathbf{K}_0 = \frac{e}{h} \begin{bmatrix} 1 & -1 \\ -1 & 1 \end{bmatrix} \tag{7.76}$$

where h is the node spacing parameter. Then, the diagonal components of the stiffness matrix for any k>0 are equal to

$$K_k^{2+2^{K-1}+J} = \frac{2^{k+1} e}{h} \tag{7.77}$$

It should be underlined that the FEM so modified reflects perfectly the needs of computational modelling of multiscale media. When the homogenisation based modelling is performed, then the effective stiffness matrix is introduced as

$$\mathbf{K}_0^{(eff)} = \frac{e^{(eff)}}{h}\begin{bmatrix} 1 & -1 \\ -1 & 1 \end{bmatrix} \tag{7.78}$$

and in practice there is no need for a wavelet decomposition of this matrix. We observe that the projection algorithm can be applied for such $n \in N$ that ensure a sufficient mesh zoom on the smallest scale details in the composite microstructure.

The effectiveness of this approach can be illustrated with the following projection on the wavelet space for the function $f(t) = \cos(2\pi t)$ where $t \in [0,1]$ performed by use of the symbolic computation package MAPLE [70,182]. It is done for n=2,…,7 and is presented correspondingly in Figures 7.16−7.21 below with computational performance indices collected in Table 7.1 (valid for a COMPAQ 475 MHz). As is observed, the increasing projection order decisively increases the computational time of wavelet decomposition of a multiscale phenomenon necessary for the FEM approach.

Table 7.1. Computational symbolic projection of cosine wavelets

Projection order 'n'	**Finite elements number**	**Computational time [sec]**	**Memory[MB]**
2	4	3.9	2.00
3	8	8.0	2.31
4	16	11.1	2.69
5	32	23.9	3.37
6	64	48.6	4.62
7	128	132.1	7.12

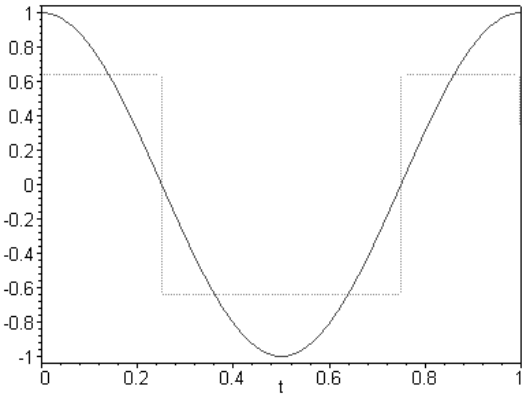

Figure 7.16. Wavelet projection for n=2

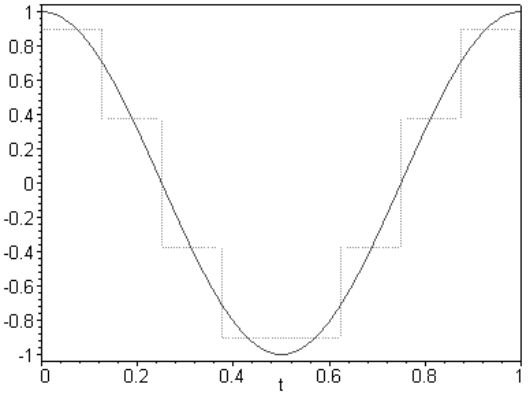

Figure 7.17. Wavelet projection for n=3

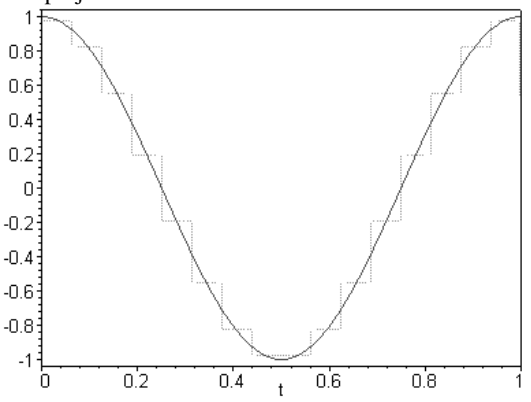

Figure 7.18. Wavelet projection for n=4

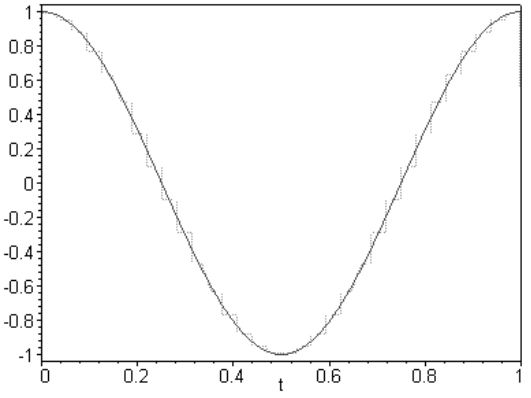

Figure 7.19. Wavelet projection for n=5

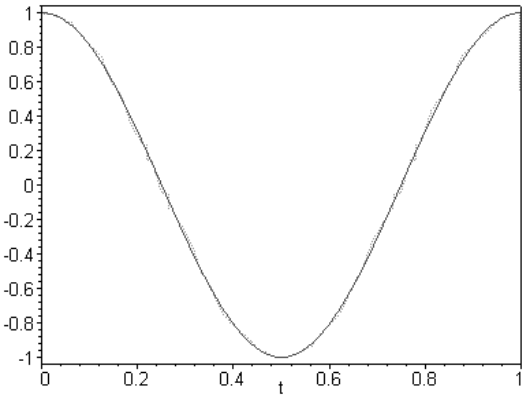

Figure 7.20. Wavelet projection for n=6

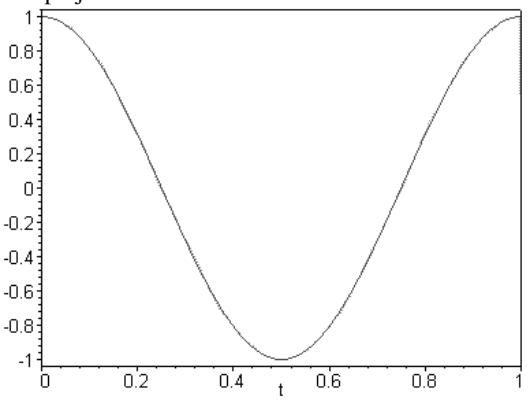

Figure 7.21. Wavelet projection for n=7

Computational experiments are performed using the system MAPLE and the additional implementation of the multiresolution homogenisation analysis. Basic computations are carried out with respect to interrelations between physical constants of both layers as well as the expansion order. Furthermore, deterministic and stochastic sensitivities of complex effective parameters (real and imaginary parts) are computed with respect to the first probabilistic moments of input physical parameters of composite layers. Finally, let us observe that a homogenised system, both in terms of deterministic or stochastic effective coefficients, can be analysed numerically using a classical Finite Element Method (FEM), for instance, or by application of various stochastic numerical methods (simulation, perturbation-based or spectral). A homogenisation–based numerical approach will considerably speed up the process of computational modelling of composites and, in the case of very complicated multiscale heterogeneous media, it can be the only available method.

7.5 Free Vibrations Analysis

The main idea of homogenisation problem solution now is a separate calculation of the effective elastic modulus and spatial averaging of the mass density, where the first part only needs multiresolutional approach [189]. The alternative wavelet−based methodology is presented in [328,329], for a plate wave propagation in [152], whereas some classical unidirectional examples are contained in [330]. Let us consider the following differential equilibrium equation:

$$-\frac{d}{dx}\left(e(x)I(x)\frac{d}{dx}u(x)\right)=M(x)\,;\quad x\in[0,1] \tag{7.79}$$

where $e(x)$, defining material properties of the heterogeneous medium, varies arbitrarily on many scales together with the inertia momentum $I(x)$. A multiresolutional homogenisation starts now from the following decomposition of the equilibrium equation:

$$\begin{cases}\dfrac{d}{dx}v(x)=-M(x)\\ \dfrac{d}{dx}u(x)=\dfrac{v(x)}{e(x)I(x)}\end{cases} \tag{7.80}$$

to determine the homogenised coefficient $e^{(eff)}$ constant over the interval $x\in[0,1]$, which takes the integral form

$$\begin{pmatrix}u(x)\\ v(x)\end{pmatrix}-\begin{pmatrix}u(0)\\ v(0)\end{pmatrix}=\int_0^x\left(\begin{pmatrix}0 & e(t)^{-1}I(t)^{-1}\\ 0 & 0\end{pmatrix}\begin{pmatrix}u(t)\\ v(t)\end{pmatrix}+\begin{pmatrix}0\\ -M(t)\end{pmatrix}\right)dt \tag{7.81}$$

On the other hand, the reduction algorithm between multiple scales of the composite consists in determination of such effective tensors $B^{(eff)}$, $A^{(eff)}$, $p^{(eff)}$ and $q^{(eff)}$, such that

$$\left(I+B^{(eff)}\right)\begin{pmatrix}u(x)\\ v(x)\end{pmatrix}+q^{(eff)}+\lambda=\int_0^x\left(A^{(eff)}\begin{pmatrix}u(t)\\ v(t)\end{pmatrix}+p^{(eff)}\right)dt \tag{7.82}$$

It can be shown that

$$B^{(eff)}=\begin{pmatrix}0 & 0\\ 0 & 0\end{pmatrix};\ A^{(eff)}=\begin{pmatrix}0 & C_1-2C_2\\ 0 & 0\end{pmatrix} \tag{7.83}$$

where

$$C_1 = \int_0^1 \frac{dt}{e(t)I(t)}; C_2 = \int_0^1 \frac{\left(t-\frac{1}{2}\right)dt}{e(t)I(t)} \tag{7.84}$$

Furthermore, for $f(x)=0$ there holds $p^{(eff)} = q^{(eff)} = 0$, while, in a general case, $B^{(eff)}$ and $A^{(eff)}$ do not depend on p and q. Finally, the homogenised ODEs are obtained as

$$\begin{cases} \dfrac{d}{dx} v(x) = f^{(eff)} \\ \dfrac{d}{dx} u(x) = \left(C_1 - 2C_2\right) v(x) \end{cases} \tag{7.85}$$

which is essentially different to the classical result of the asymptotic homogenisation shown previously. Effective mass density of a composite can be derived by a spatial averaging method, which is completely independent from the space configuration and periodicity conditions of a composite structure. The relation is used for classical and wavelet–based homogenisation approaches as well. Finally, the following variational equation is proposed to achieve the dynamic equilibrium for the linear elastic system [208]:

$$\int_\Omega \rho \ddot{u}_i \delta u_i d\Omega + \int_\Omega C_{ijkl} \varepsilon_{ij} \delta \varepsilon_{kl} d\Omega = \int_\Omega \rho f_i \delta u_i d\Omega + \int_{\partial\Omega_\sigma} \hat{t}_i \delta u_i d(\partial\Omega) \tag{7.86}$$

where u_i represents displacements of the system Ω with elastic properties and mass density defined by the elasticity tensor $C_{ijkl}(x)$ and the function ρ=ρ(**x**); the vector $\hat{t}_i$ denotes the stress boundary conditions defined on $\partial\Omega_\sigma \subset \partial\Omega$.

An analogous equation rewritten for the homogenised heterogeneous medium has the following form:

$$\int_\Omega \rho^{(eff)} \ddot{u}_i \delta u_i d\Omega + \int_\Omega C_{ijkl}^{(eff)} \varepsilon_{ij} \delta \varepsilon_{kl} d\Omega = \int_\Omega \rho^{(eff)} f_i \delta u_i d\Omega + \int_{\partial\Omega_\sigma} \hat{t}_i \delta u_i d(\partial\Omega) \tag{7.87}$$

where all material properties of the real system are replaced with the effective parameters. Let us introduce a discrete representation of the function u_i by the following vector of the generalised coordinates for the needs of the Finite Element Method implementation:

$$u_i(x) = \phi_{i\alpha}(x) q_\alpha = \left[\sum_{e=1}^{E} \phi_{i\alpha}^{(e)}(x) \right] q_\alpha \tag{7.88}$$

which gives us for the strain tensor components

$$\varepsilon_{ij}(x)=\frac{1}{2}\left[\phi_{i\alpha,j}(x)+\phi_{j\alpha,i}(x)\right]q_\alpha = B_{ij\alpha}(x)\,q_\alpha \tag{7.89}$$

The matrix description for stiffness, mass, damping components as well as the RHS vector is proposed as

$$K_{\alpha\beta}=\int_\Omega C_{ijkl}B_{ij\alpha}B_{kl\beta}\,d\Omega\,,\quad K^{(eff)}_{ijkl}=\int_\Omega C^{(eff)}_{ijkl}B_{ij\alpha}B_{kl\beta}\,d\Omega \tag{7.90}$$

$$M_{\alpha\beta}=\int_\Omega \rho\phi_{i\alpha}\phi_{i\beta}\,d\Omega\,,\quad M^{(eff)}_{\alpha\beta}=\int_\Omega \rho^{(eff)}\phi_{i\alpha}\phi_{i\beta}\,d\Omega \tag{7.91}$$

$$\begin{aligned} Q_\alpha &= \int_\Omega \rho f_i\phi_{i\alpha}\,d\Omega+\int_{\partial\Omega_\sigma}\hat{t}_i\phi_{i\alpha}\,d(\partial\Omega)\\ Q^{(eff)}_\alpha &= \int_\Omega \rho^{(eff)} f_i\phi_{i\alpha}\,d\Omega+\int_{\partial\Omega_\sigma}\hat{t}_i\phi_{i\alpha}\,d(\partial\Omega)\end{aligned} \tag{7.92}$$

Usually, it is assumed that the damping matrix can be decomposed into the part having the nature of body forces with the proportionality coefficient c_{M} and the rest composes the viscous stresses multiplied by the quantity c_{K}, so that

$$C_{\alpha\beta}=c_M M_{\alpha\beta}+c_K K_{\alpha\beta}\,,\quad C^{(eff)}_{\alpha\beta}=c_M M^{(eff)}_{\alpha\beta}+c_K K^{(eff)}_{\alpha\beta} \tag{7.93}$$

After such a discretisation of all the state functions and structural parameters in (7.86) and (7.87), the following matrix equation for real heterogeneous system is obtained:

$$M_{\alpha\beta}\ddot{q}_\beta+C_{\alpha\beta}\dot{q}_\beta+K_{\alpha\beta}q_\beta=Q_\alpha \tag{7.94}$$

Therefore, the equivalent homogenised dynamic equilibrium equation to be solved for the deterministic problem has the form

$$M^{(eff)}_{\alpha\beta}\ddot{\overline{q}}_\beta+C^{(eff)}_{\alpha\beta}\dot{\overline{q}}_\beta+K^{(eff)}_{\alpha\beta}\overline{q}_\beta=Q^{(eff)}_\alpha \tag{7.95}$$

where the barred unknowns represent the response of the homogenised system. The RHS vector is equal to 0, so the homogenised operators are to be computed for the LHS components only in the case of free vibrations. The eigenvalues and eigenvectors for the undamped systems are determined from the following matrix equations:

$$\left(K_{\alpha\beta}-\omega_{(\alpha)}M_{\alpha\beta}\right)\Phi_{\beta\gamma}=0\,;\quad \left(K^{(eff)}_{\alpha\beta}-\overline{\omega}_{(\alpha)}M^{(eff)}_{\alpha\beta}\right)\overline{\Phi}_{\beta\gamma}=0 \tag{7.96}$$

which are implemented and applied below to compare homogenised and real composites.

Numerical analysis illustrating presented ideas is carried out in two separate steps. First, homogenised characteristics of a periodic composite determined thanks to different homogenisation models are obtained by the use of the MAPLE symbolic computation. Then, the FEM analysis of the free vibration problems is made for the simply supported two−, three− and five−bay periodic beams, made of the original and homogenised composites, having applications in aerospace and other engineering structures subjected to vibrations [189]. The periodicity is observed in macroscale (equal length of each bay) as well as in microstructure – each bay is obtained by reproduction of the identical RVE whose elastic modulus is defined by some wavelet function.

The formulae presented above are implemented in the program MAPLE together with the spatial averaging method in order to compare the homogenised modulus computed by various ways (spatial averaging, classical and multiresolutional) for the same composite. Figure 7.22 illustrates the variability of this modulus along the RVE, where the function $e(x)$ is subtracted from the following Haar and Mexican hat wavelets:

$$h(x) = \begin{cases} 20.0E9; 0 \le x \le 0.5 \\ 2.0E9\ 0.5 < x \le 1 \end{cases} \tag{7.97}$$

$$m(x) = 2 + \frac{1}{\sqrt{2\pi}\sigma^3} \frac{x^2}{\sigma^2 - 1} \exp\left(\frac{-x^2}{2\sigma^2} \right), \ \sigma\text{=-0.4} \tag{7.98}$$

as

$$e(x) = 10.0h(x) + 2.0E9\ m(x) \tag{7.99}$$

Mass density of the composite is adopted as the wavelet of similar nature

$$\tilde{h}(x) = \begin{cases} 200; 0 \le x \le 0.5 \\ 20; 0.5 < x \le 1 \end{cases} \tag{7.100}$$

with

$$\rho(x) = 0.5\ \tilde{h}(x) + 0.5\ m(x) \tag{7.101}$$

which is displayed in Figure 7.23.

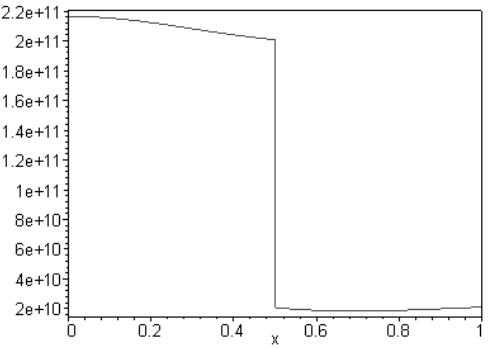

Figure 7.22. Wavelet-based definition of elastic modulus in the RVE

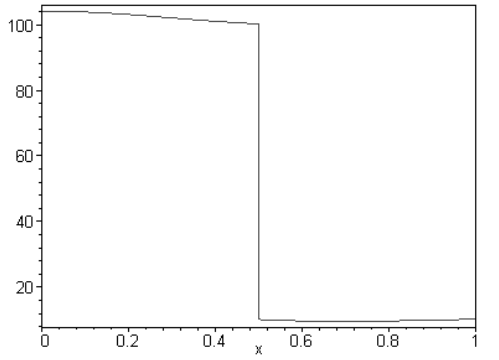

Figure 7.23. Wavelet-based definition of mass density in the RVE

The final form of these functions is established on the basis of the mathematical conditions for homogenisability analysed before as well as to obtain the final variability of composite properties similar to the traditional multi-component structures. Let us note that classical definition of periodic composite material properties contained the piecewise constant Haar basis only.

The following homogenised material properties are obtained from this input: $\rho^{(eff)} = 56.137$, $e^{(av)} = 114.548\ E9 >$ $e^{(eff,wav)} = 60.217\ E9 >$ $e^{(eff)} = 35.437\ E9$, which means that for this particular example, the highest value is obtained for the spatial averaging method, then – for the wavelet approach at least – for classical homogenisation method based on the small parameter assumption. The effectiveness of such homogenisation results is verified in the next section by comparison of the eigenvalues and the eigenfunctions of some periodic composite beams being homogenised with its real material distribution.

The free vibration problems for two−, three− and five−bay periodic beams are solved using the classical and homogenisation−based Finite Element Method implementation [13,387]. The unitary inertia momentum is taken in all computational cases, ten periodicity cells compose each bay, while material properties inserted in the numerical model are calculated from (a) spatial averaging, (b) the classical homogenisation method and (c) the multiresolutional

scheme proposed above and compared against the real structure response. The results of eigenproblem solutions are presented as the first 10 eigenvalue variations for the beams in Figures 7.24, 7.26 and 7.28 together with the maximum deflections of these beams in Figures 7.25, 7.27 and 7.29 – the resulting values are marked on the vertical axes, while the number of the eigenvalue being computed is on the horizontal axes. The particular solutions for 1st, 2nd, 3rd and lower next eigenvalues are connected with the continuous lines to better illustrate interrelations between the results obtained in various homogenisation approaches related to the real composite model.

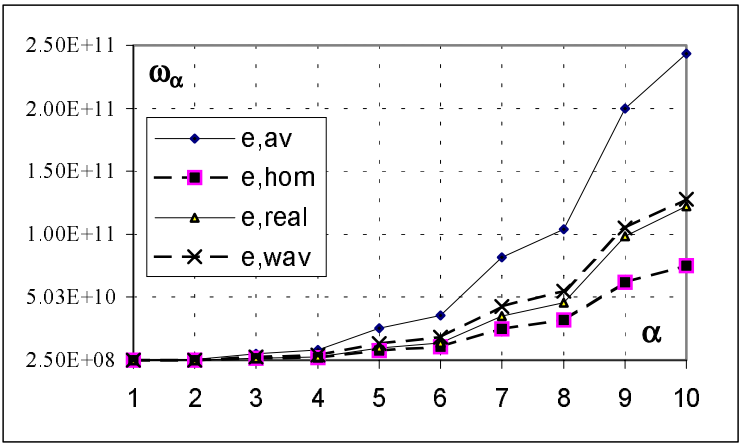

Figure 7.24. Eigenvalues progress for various two−bay composite structures

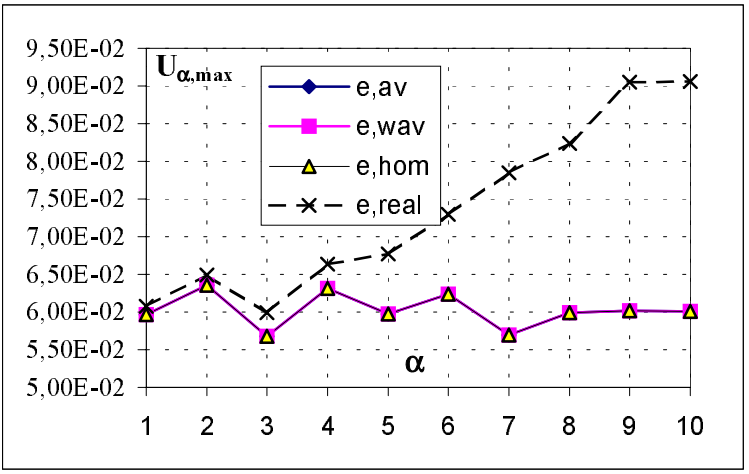

Figure 7.25. Maximum deflections for the eigenproblems of two−bay composite structures

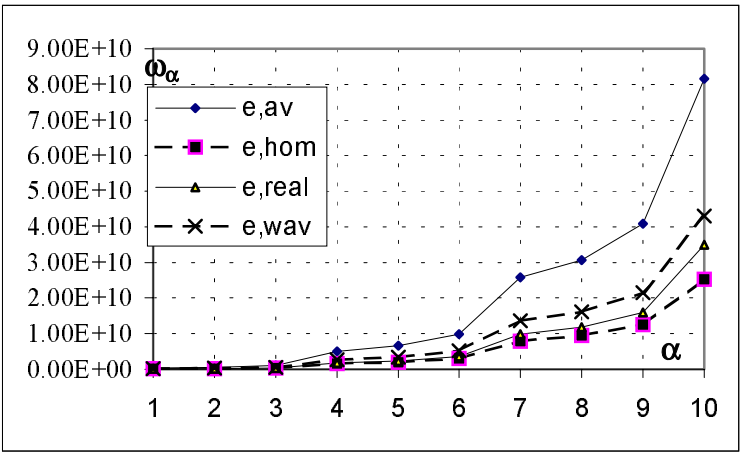

Figure 7.26. Eigenvalues progress for various three−bay composite structures

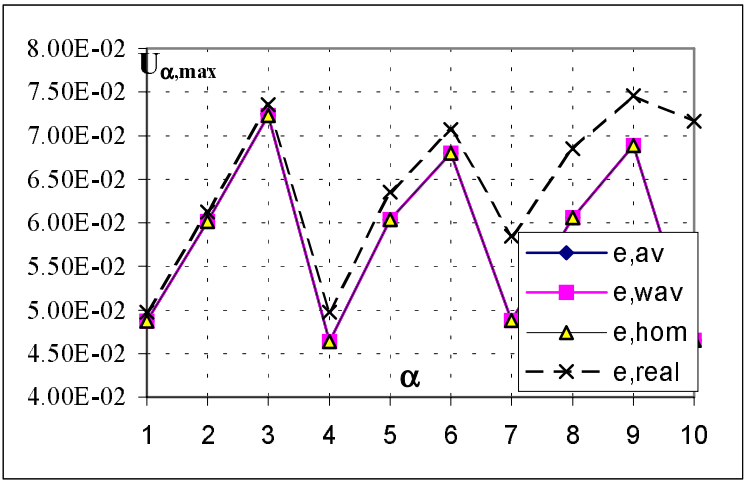

Figure 7.27. Maximum deflections for the eigenproblems of three−bay composite structures

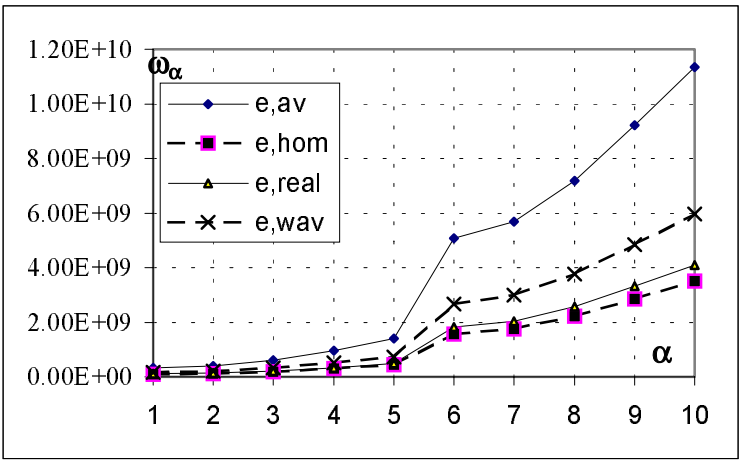

Figure 7.28. Eigenvalues progress for various five–bay composite structures

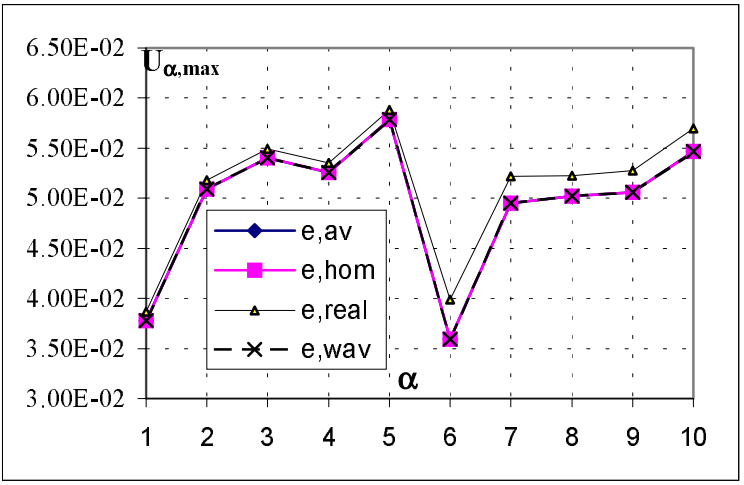

Figure 7.29. Maximum deflections for the eigenproblems of five–bay composite structures

As can be observed, the eigenvalues obtained for various homogenisation models approximate the values computed for the real composite with different accuracies, and the maximum deflections are the same. The weakest efficiency in eigenvalue modelling is detected in the case of a spatially averaged composite – the difference in relation to the real structure results increases together with the eigenvalue number. Wavelet–based and classical homogenisation methods give more accurate results – the first method is better for smaller numbers of bays (and the RVEs along the beam) see Figure 7.24, whereas the classical homogenisation approach is recommended in the case of increasing number of the bays and the RVEs, cf. Figures 7.26 and 7.28. The justification of this observation comes from the fact that the wavelet function appears to be of less importance for the

increasing number of periodicity cells in the structure. Another interesting result is that the efficiency of the approximation of the maximum deflections for a multibay periodic composite beam by the deflections encountered for homogenised systems increases together with an increase of the total number of bays. The agreement between the eigenvalues for the real and homogenised systems will allow usage of the stochastic spectral finite element techniques [261], where the random process expansions are based on the relevant eigenvalues.

Finally, let us note that further extensions of this model on vibration analysis of fibre-reinforced composites [60] using 2D wavelets are possible. An application of wavelet technique is justified by the fact that the spatial distribution of the constituents in the composite specimen is recently a subject of digital image analysis [341]. On the other hand, chaotic behaviour of real and homogenised composites [199] may be studied in the above context.

7.6 Multiscale Heat Transfer Analysis

The idea of transient heat transfer homogenisation, i.e. calculation of the effective material parameters, consists in separate spatial averaging of the volumetric heat capacity and the solution (analytical or numerical) of the heat conduction homogenisation problem [15,165,166,195]. As is illustrated below, the final form of the effective heat conductivity coefficient varies with the composite model, whereas a composite with piecewise constant properties and/or defined by some wavelet functions can have the same homogenised volumetric heat capacity. That is why first the heat conduction equation for a 1D periodic composite is homogenised and the effective heat capacity and mass density are determined by a spatial averaging approach. The multiresolutional homogenisation method starts from the following decomposition of heat conduction equation [23,55] as follows:

$$\begin{cases} \dfrac{d}{dx} v(x) = -Q(x) \\ \dfrac{d}{dx} T(x) = \dfrac{v(x)}{k(x)} \end{cases} \tag{7.102}$$

The main goal is to determine the homogenised coefficient $k^{(eff)}$ being constant over the interval $x \in [0,1]$. Therefore, the equation system (7.102) can be rewritten as

$$\begin{pmatrix} T(x) \\ v(x) \end{pmatrix} - \begin{pmatrix} T(0) \\ v(0) \end{pmatrix} = \int_0^x \left(\begin{pmatrix} 0 & k(t)^{-1} \\ 0 & 0 \end{pmatrix} \begin{pmatrix} T(t) \\ v(t) \end{pmatrix} + \begin{pmatrix} 0 \\ -Q(t) \end{pmatrix} \right) dt \tag{7.103}$$

On the other hand, the reduction algorithm between multiple scales of the composite consists in the determination of such effective operators $B^{(eff)}$, $A^{(eff)}$, $p^{(eff)}$, $q^{(eff)}$, that

$$\left(I + B^{(eff)}\right)\begin{pmatrix} T(x) \\ v(x) \end{pmatrix} + q^{(eff)} + \lambda = \int_0^x \left(A^{(eff)} \begin{pmatrix} T(t) \\ v(t) \end{pmatrix} + p^{(eff)} \right) dt \tag{7.104}$$

It can be shown that

$$B^{(eff)} = \begin{pmatrix} 0 & 0 \\ 0 & 0 \end{pmatrix}; A^{(eff)} = \begin{pmatrix} 0 & k_1 - 2k_2 \\ 0 & 0 \end{pmatrix} \tag{7.105}$$

where

$$k_1 = \int_0^1 \frac{dt}{k(t)}; k_2 = \int_0^1 \frac{\left(t - \frac{1}{2}\right) dt}{k(t)} \tag{7.106}$$

Furthermore, for $Q(x)$=0 there holds $p^{(eff)} = q^{(eff)} = 0$ (in a general case, $B^{(eff)}$ and $A^{(eff)}$ do not depend on p and q). Finally, the system of two homogenised ordinary differential equations are obtained as

$$\begin{cases} \dfrac{d}{dx} v(x) = q^{(eff)} \\ \dfrac{d}{dx} T(x) = \left(k_1 - 2k_2\right) v(x) \end{cases} \tag{7.107}$$

which is essentially different than the classical result of the asymptotic homogenisation shown previously. Let us observe that in the case of the heat conductivity variability in two separate scales $k = k\left(x, \dfrac{x}{\varepsilon}\right)$ the multiresolutional scheme reduces to the classical macro–micro methodology where the following limits are demonstrated:

$$\lim_{\varepsilon \to 0} k_1(\varepsilon) = k_1 \quad \text{and} \quad \lim_{\varepsilon \to 0} k_2(\varepsilon) = 0 \tag{7.108}$$

Finally, the effective volumetric heat capacity of a composite is determined by the spatial averaging method, which relation does not depend either on the space configuration or on the periodicity conditions of a composite structure, and is used for both classical and multiresolutional homogenisation approaches.

Using traditional FEM discretisation of the temperature field and its gradients by the nodal temperatures vector θ_α [7,21,213,283]

$$T(y) = H_\alpha(y)\theta_\alpha \; ; \quad \alpha=1,...,N \tag{7.109}$$

$$T_{,y}(y) = H_{\delta,y}(y)\theta_\delta \; ; \quad \delta=1,...,N \tag{7.110}$$

the following transient problems are solved:

- averaged material properties

$$C^{(av)}_{\delta\beta}\dot{\theta}'_\beta + K^{(av)}_{\delta\beta}\theta'_\beta = P^{(av)}_\delta , \quad \delta,\beta = 1,2,...,N , \tag{7.111}$$

- asymptotically homogenised material properties

$$C^{(eff)}_{\delta\beta}\dot{\theta}''_\beta + K^{(eff)}_{\delta\beta}\theta''_\beta = P^{(eff)}_\delta , \quad \delta,\beta = 1,2,...,N , \tag{7.112}$$

- for multiresolutionally homogenised material properties in the system

$$C^{(eff)w}_{\delta\beta}\dot{\theta}'''_\beta + K^{(eff)w}_{\delta\beta}\theta'''_\beta = P^{(eff)w}_\delta , \quad \delta,\beta = 1,2,...,N . \tag{7.113}$$

Numerical analysis illustrating the ideas presented is carried out in two separate steps. First, homogenised characteristics of a periodic composite obtained through different homogenisation models are determined by the use of MAPLE symbolic computations. This numerical approach is used also to verify input parameter variability of the homogenised characteristics as well as design sensitivities of these characteristics with respect to the contrast parameter (interrelation between the heat conductivities of the composite components) and the interface location along the RVE length (g). Next, the FEM analysis of transient heat transfer is made to discuss the differences between temperature and heat flux histories resulting from various homogenisation models contrasted with the real system. An alternative way to model multiscale transient heat transfer phenomena in composites is to expand the classical FEM methodology using a wavelet based both space and time adaptive numerical methods, as it was discussed in [17], for instance; the other aspects of this problem have been studied in [40].

The formulae for effective heat conductivity are implemented in the program MAPLE together with the spatial averaging method in order to compare the homogenised modulus computed by various ways for the same composite. Figure 7.30 illustrates the variability of this modulus along the RVE, where the function $k(x)$ is subtracted from the following Haar basis and Mexican hat wavelet:

$$h(x) = \begin{cases} k_1 ; 0 \le x \le 0.5 \\ k_2 ; 0.5 < x \le 1 \end{cases} \tag{7.114}$$

$$m(x) = 2 + \frac{1}{\sqrt{2\pi}\sigma^3}\frac{x^2}{\sigma^2 - 1}\exp\left(\frac{-x^2}{2\sigma^2}\right), \quad \sigma\text{=-0.5} \tag{7.115}$$

as

$$k(x) = h(x) + 0.001\, m(x) \tag{7.116}$$

Further, volumetric heat capacity of the composite is adopted as the wavelet of a similar form

$$\tilde{h}(x) = \begin{cases} \rho_1 c_1;\ 0 \le x \le 0.5 \\ \rho_2 c_2;\ 0.5 < x \le 1 \end{cases} \tag{7.117}$$

with

$$\rho(x)c(x) = \tilde{h}(x) + 10^3\, m(x) \tag{7.118}$$

which is demonstrated in Figure 7.31.

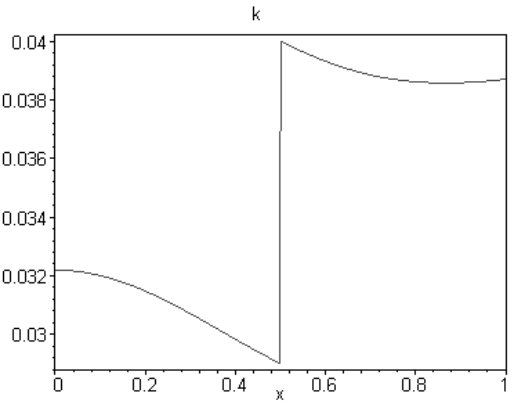

Figure 7.30. Wavelet-based definition of heat conductivity coefficient in RVE

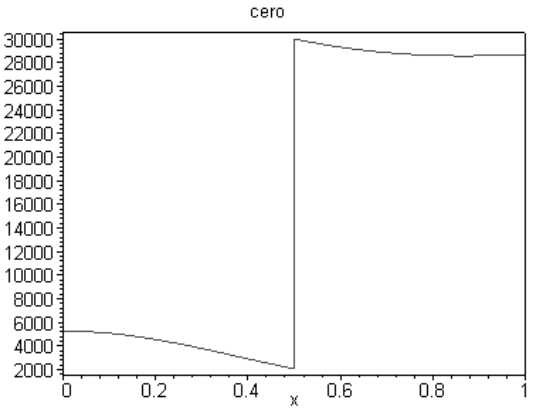

Figure 7.31. Wavelet-based definition of the volumetric heat capacity in RVE

The final form of these functions is established on the basis of the mathematical conditions for homogenisability analysed before as well as to obtain the final variability of composite properties similar to the traditional multi-component structures. Let us note that the classical definition of periodic composite material properties contained the piecewise constant Haar basis only.

Symbolic computations of the MAPLE system were used next to perform the comparison between the spatial averaging, classical and multiresolutional homogenisation scheme for various values of the composite constituents contrast and the interface position g. The results of the analysis are demonstrated in Figures 7.32, 7.33 and 7.34, respectively. However it could be expected, the results of spatial averaging are globally the greatest for the entire variability ranges of the design parameters, while the interrelation between the classical and wavelet-based methods differ on the input parameter values.

The separate, very interesting numerical problem would be to determine the intersection of the surfaces plotted in Figures 7.33 and 7.34. It can be interpreted as the curve equivalent to such pairs of the contrast and interface location in the RVE for which both multiresolutional and classical homogenisation methods can result in the same effective quantity. Let us note that the problem is independent from physical interpretation of homogenised characteristics).

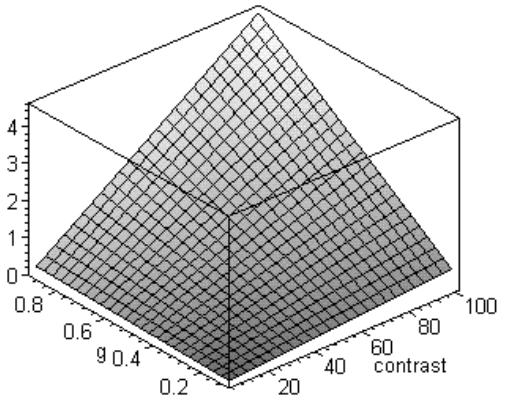

Figure 7.32. Parameter variability of $k^{(av)}$

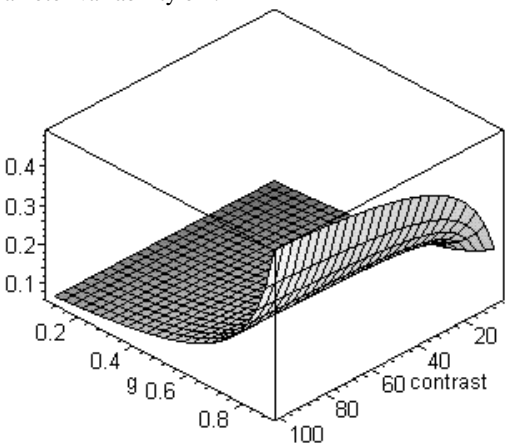

Figure 7.33. Parameter variability of $k^{(eff)}$

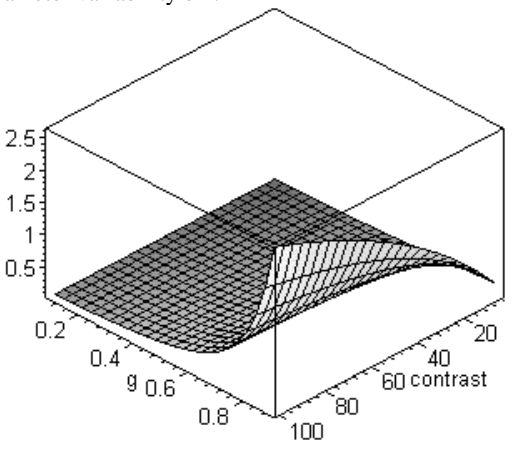

Figure 7.34. Parameter variability of $k^{(eff)w}$

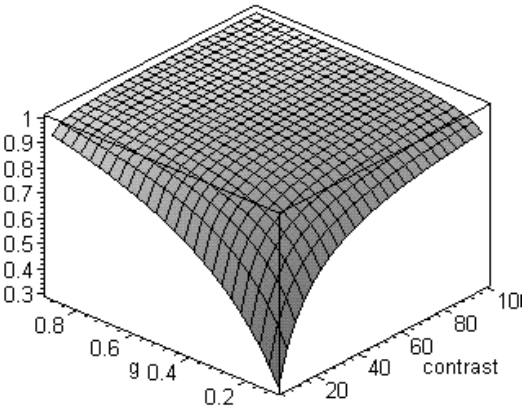

Figure 7.35. Sensitivity of $k^{(av)}$ wrt contrast parameter

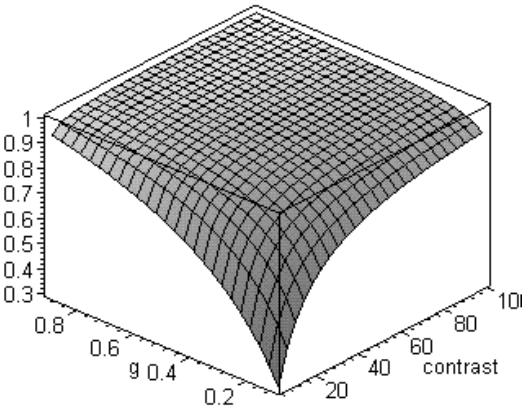

Figure 7.36. Sensitivity of $k^{(av)}$ wrt the interface location

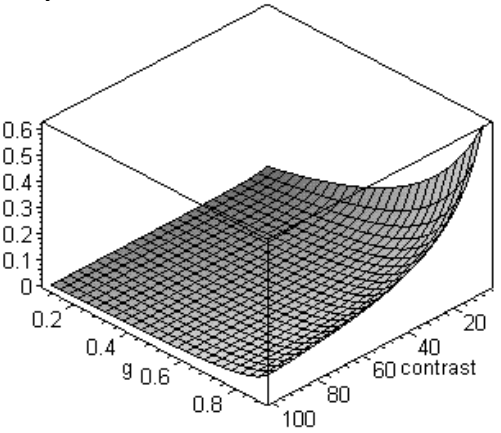

Figure 7.37. Sensitivity of $k^{(eff)}$ coefficient wrt components contrast

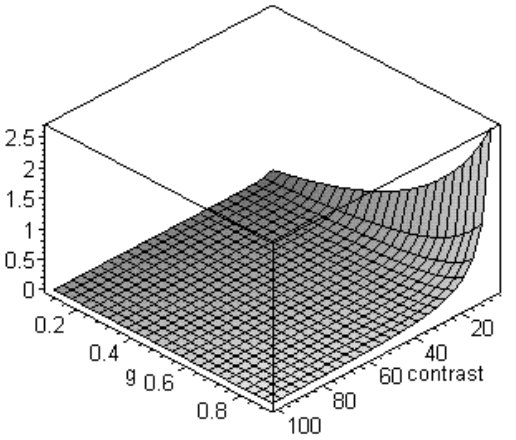

Figure 7.38. Sensitivity of $k^{(eff)}$ wrt interface location

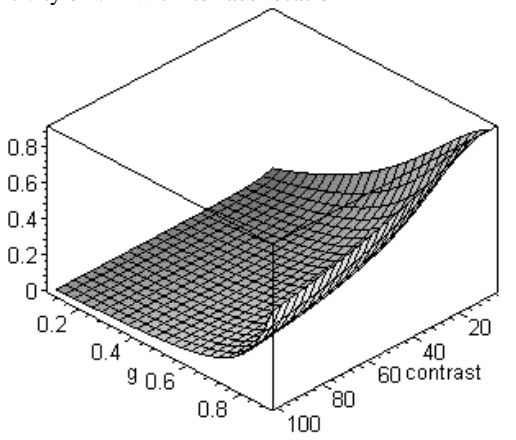

Figure 7.39. Parameter sensitivity of $k^{(eff)w}$ wrt contrast parameter

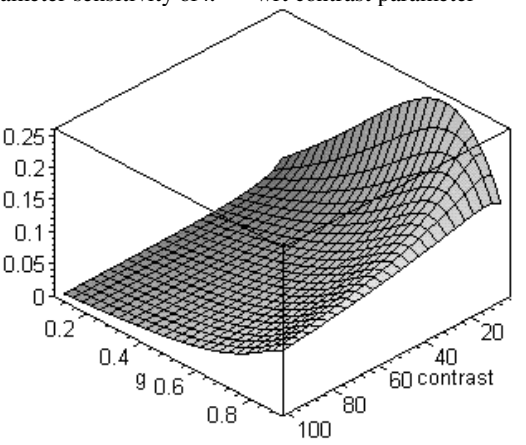

Figure 7.40. Parameter sensitivity of $k^{(eff)w}$ wrt interface location

Partial derivatives of the averaged, asymptotically and multiresolutionally homogenised heat conductivity are normalised using the factor h/k where h denotes the contrast or the parameter g, while $k \equiv \{k^{(av)}, k^{(eff)}, k^{(eff)w}\}$. The results of symbolic computations are presented in Figures 7.35−7.40 and it is clear that the spatial averaging method results in the composite with an extremely different parameter sensitivity in comparison to the other homogenisation models (both quantitatively and qualitatively). Sensitivity gradients for asymptotic and multiresolutional homogenisations have very analogous surfaces – the only differences are observed for higher values of the design parameters. The numerical results obtained can be effectively used in the optimisation of composite materials according to the methodology based on the homogenisation approach. Moreover, they can be applied to the homogenisation of random composites where first and second order parameter sensitivities are necessary to determine the first two probabilistic moments of the effective parameter in the second order perturbation approach at least.

The transient heat transfer phenomenon in a two−layer unidirectional composite structure has been modelled using the commercial Finite Element Method program ANSYS [2]. The division of the periodicity cell with unit length L=1.0 m into two components with equal lengths and 1000 of 4−noded isoparametric heat transfer finite elements PLANE55 (500 elements for each material) is schematically shown in Figure 7.41. Constant temperature T=0 is applied at the left boundary and the unit heat flux Q at the right edge, whereas initial temperatures along the composite are taken as equal to 0. Material properties used in numerical analysis are calculated for (a) real composite structure – test no 1, (b) spatially averaged composite – test no 2, (c) classical homogenisation method – test no 3, and (d) multiresolutional homogenisation scheme proposed now – test no 4. Input material data for particular computational tests are collected in Table 7.2 below.

Table 7.2. Material data for the FEM analysis

Computational test number	***k* [W/m°C]**	***c* [J/kg°C]**
1	0.031 / 0.0385	4000 / 29000
2	0.0349	16465.20
3	0.0345	16465.20
4	0.0328	16465.20

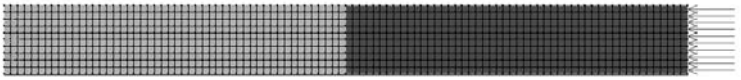

Figure 7.41. Finite Element mesh for the composite structure

The results for the steady−state analysis are shown in Figures 7.42−7.45 in the form of a spatial temperature distribution and the analogous heat flux distribution along the composite; their error approximations are computed and visualised also.

Considering the nonstationary character of the transient heat transfer, the temperature distributions for various moments of the heating process are collected in Figures 7.46–7.53. Analysing the temperatures fields along the composite structure it can be observed that the best agreement with the structural behaviour is obtained for the test related to the multiresolutionally homogenised composite. The classical homogenisation method gives more accurate results in the neighbourhood of the heated surface only. In the case of temperature gradients it can be concluded that the wavelet–based homogenisation approach gives the highest averages temperature gradient and greater than the classical method and spatial averaging, respectively. It is important considering reliability analysis based on the homogenisation methods; this gradient is however a few percent smaller than the maximum gradient for the real composite.

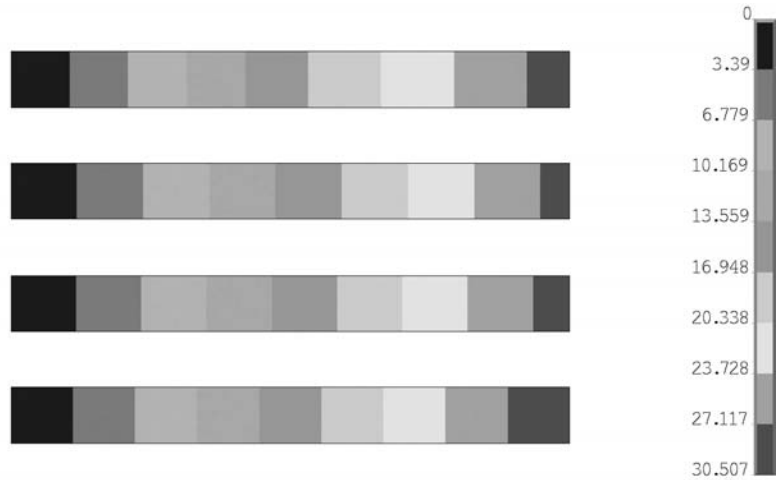

Figure 7.42. Spatial distribution of temperatures in composite

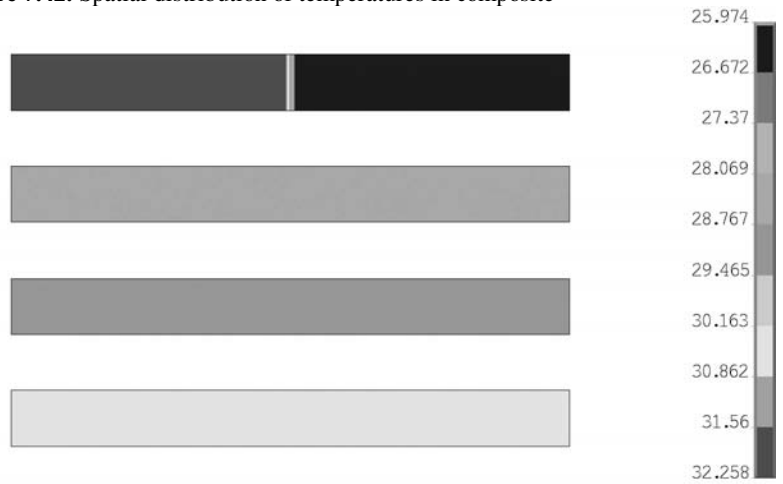

Figure 7.43. Temperature gradients along the composite

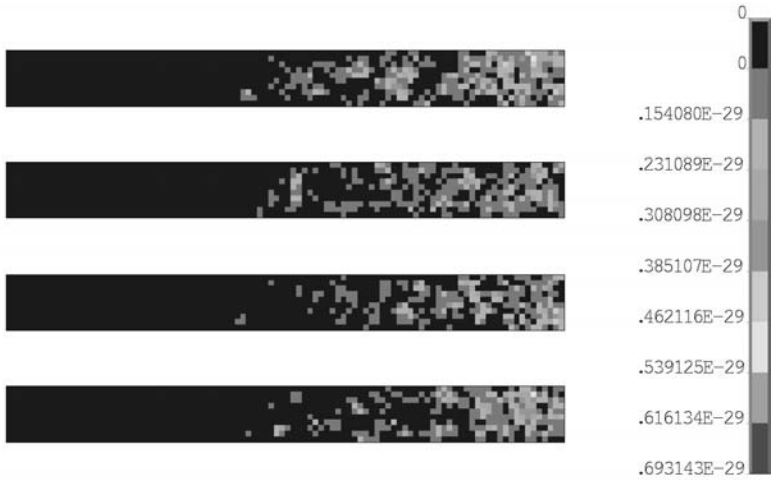

Figure 7.44. Solution error distribution along the composite

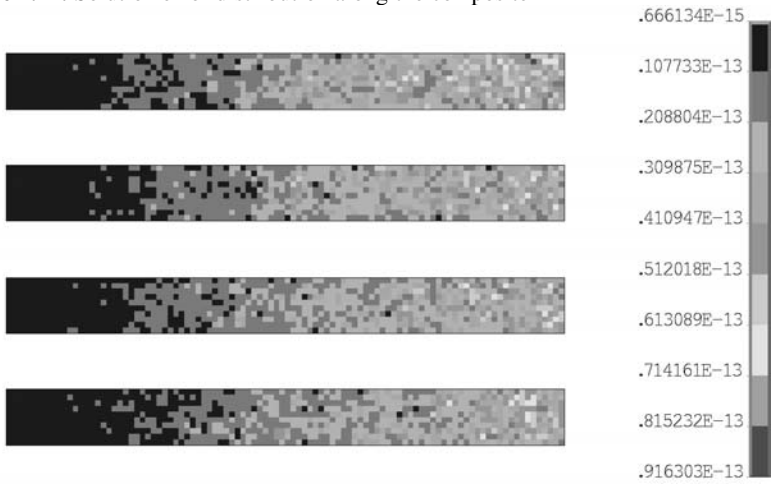

Figure 7.45. Temperature gradient error along the composite

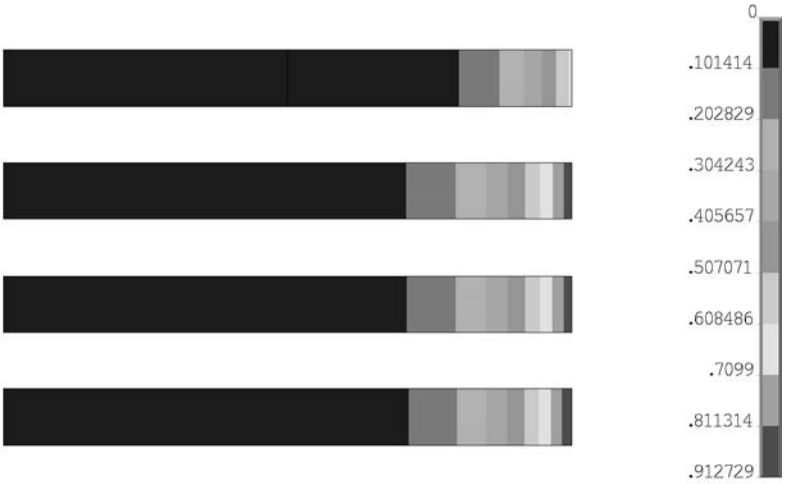

Figure 7.46. Temperature distribution for t=2x10 E4 sec

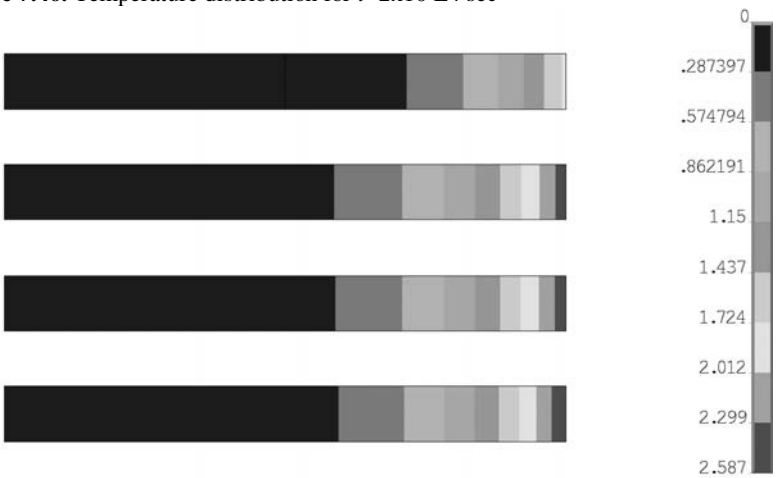

Figure 7.47. Temperature distribution for t=4x10 E4 sec

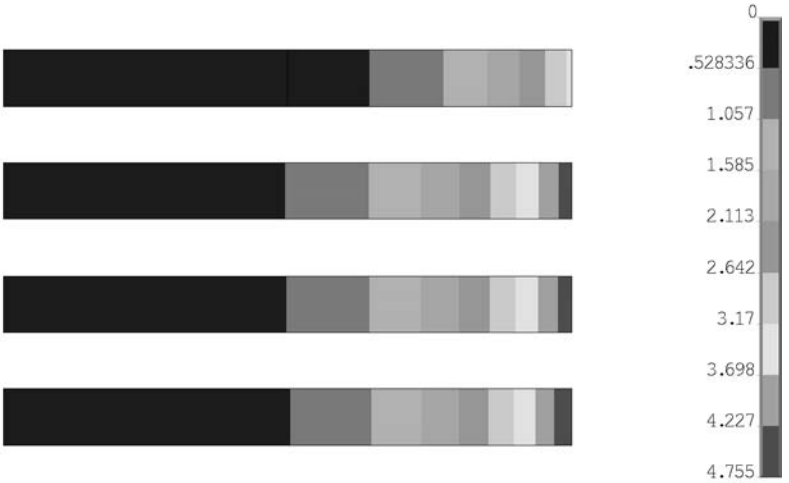

Figure 7.48. Temperature distribution for t=5x10 E4 sec

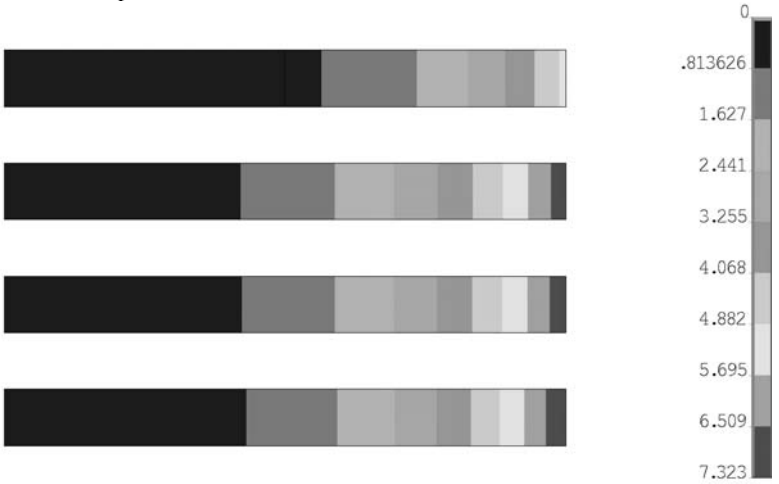

Figure 7.49. Temperature distribution for t= 8x10 E4 sec

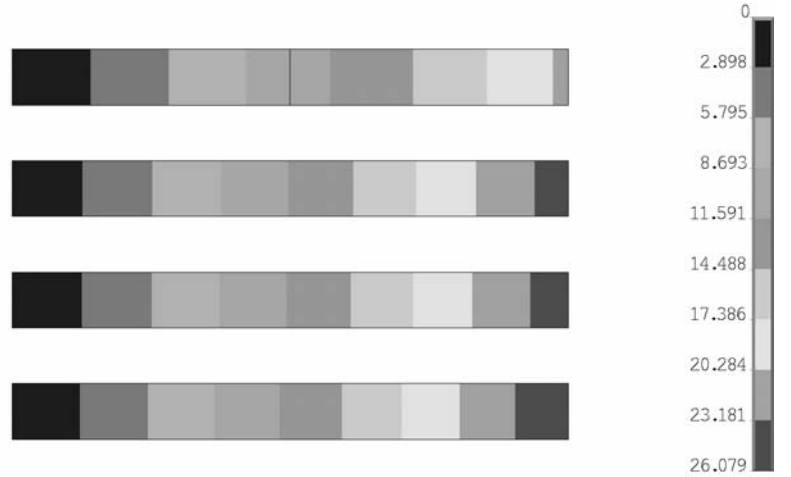

Figure 7.50. Temperature distribution for t= 4x10 E5 sec

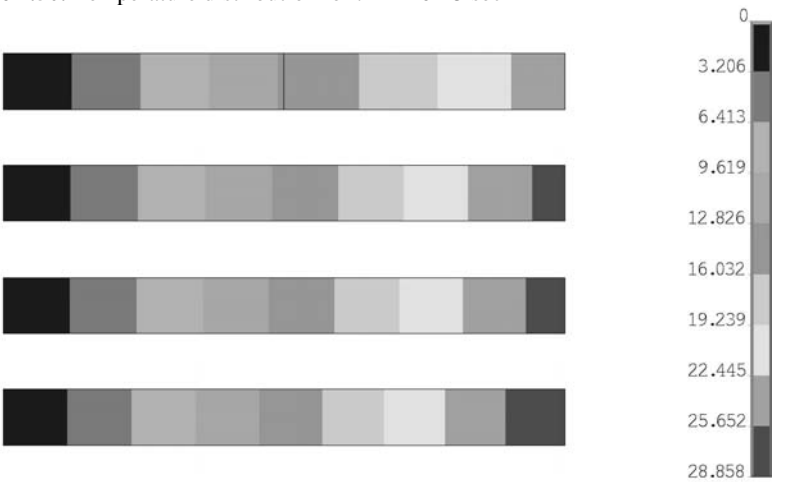

Figure 7.51. Temperature distribution for t=6x10 E5 sec

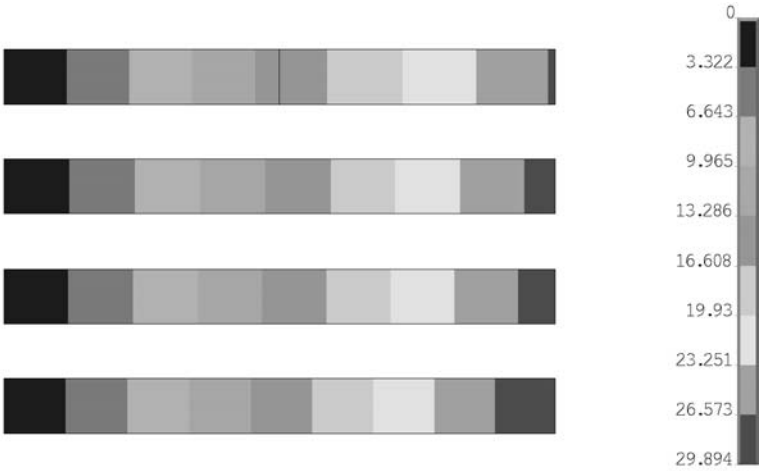

Figure 7.52. Temperature distribution for t=8x10 E5 sec

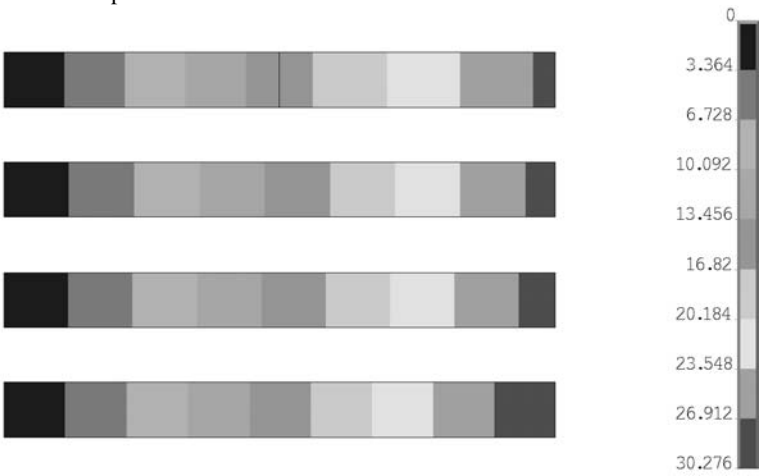

Figure 7.53. Temperature distribution for t=1x10 E6 sec

The temperature solution error related to the real composite behaviour numerical tests is best approximated by the error computed for the structure homogenised by the wavelet–based methodology also – it shows analogous spatial distribution and maximum values, although spatial distribution is analogous in all cases as well. In further analysis the results obtained should be contrasted with the implementation of the wavelet decomposition of initial material properties in the Finite Element Method program.

Finally, transient behaviour of the composite is analysed numerically and presented for various time moments of the heating process in Figures 7.46–7.53. The real composite is heated at the boundary relevant to the material with higher volumetric heat capacity and the contrast between heat capacities is very high. That is why the heating process in the real composite is very slow – significantly slower than takes place in all homogenised models (Figure 7.53 corresponds to almost a

steady state for comparison). The opposite relation can be noticed in the case of inverted materials in the analysed laminate. Neglecting temperature scale differences between the real and effective models, the best approximation for the original structure behaviour is done by the spatially averaged system.

7.7 Stochastic Perturbation–based Approach to the Wavelet Decomposition

Let us consider a multiresolutional wavelet–based algorithm and its application in the solution of the linear algebraic equations system [334] being a basis for various discrete numerical techniques [206]. There holds

$$\mathbf{Kq} = \mathbf{f} \tag{7.119}$$

where the matrix K is positive definite and represents the behaviour of some linear engineering system, q is a discretised vector of the engineering system response resulting from the excitation expressed by a vector f. Further, let us assume for the needs of the algorithm applicability, that matrix $\mathbf{K}$ is of the size 2^nx2^n and let us introduce the Haar transform for the vector $\mathbf{q}$ in the following way:

$$\mathbf{s}^{(k)} = \frac{1}{\sqrt{2}}\left(\mathbf{q}^{(2k-1)} + \mathbf{q}^{(2k)}\right) \tag{7.120}$$

$$\mathbf{d}^{(k)} = \frac{1}{\sqrt{2}}\left(\mathbf{q}^{(2k-1)} - \mathbf{q}^{(2k)}\right) \tag{7.121}$$

with k=1,...,2^{n-1}. Let us observe that $\mathbf{s}^{(k)}$ are introduced to scale averages of the vector $\mathbf{q}$ values in the neighbouring points while $\mathbf{d}^{(k)}$ is to scale their differences. Let us introduce the matrix M_n such that

$$\mathbf{M} = M_n = \frac{1}{\sqrt{2}}\begin{bmatrix} 1 & 1 & 0 & 0 & & & \dots \\ 0 & 0 & 1 & 1 & 0 & 0 & \dots \\ & & & & & & \dots \\ 1 & -1 & 0 & 0 & & & \dots \\ 0 & 0 & 1 & -1 & 0 & 0 & \dots \\ & & & & & & \dots \\ \dots & \dots & \dots & \dots & \dots & \dots & \dots \end{bmatrix} \tag{7.122}$$

having dimensions 2^nx2^n and such that

$$M_n^T M_n = M_n M_n^T = I \tag{7.123}$$

whose top half is denoted by L_n, while the bottom one is H_n. Then, the orthogonality gives

$$M_n^T M_n = H_n^T H_n + L_n^T L_n = I \tag{7.124}$$

and

$$H_n^T H_n = I\,,\ L_n^T L_n = I \tag{7.125}$$

where

$$\mathbf{Lq} = \mathbf{s}\,,\quad \mathbf{Hq} = \mathbf{d} \tag{7.126}$$

Let us rewrite (7.119) in the form of a pair of equations with unknown **s** and **d** as follows:

$$\mathbf{LKq} = \left(\mathbf{LKL}^T\right)\mathbf{Lq} + \left(\mathbf{LKH}^T\right)\mathbf{Hq} = \mathbf{Lf} \tag{7.127}$$

Similarly, there holds

$$\mathbf{HKq} = \left(\mathbf{HKL}^T\right)\mathbf{Lq} + \left(\mathbf{HKH}^T\right)\mathbf{Hq} = \mathbf{Hf} \tag{7.128}$$

Denoting further by

$$\mathbf{LKL}^T = \mathbf{T}, \mathbf{LKH}^T = \mathbf{C} \tag{7.129}$$

and

$$\mathbf{HKL}^T = \mathbf{B}, \mathbf{HKH}^T = \mathbf{A} \tag{7.130}$$

as well as

$$\mathbf{Lf} = \mathbf{f}_s, \mathbf{Hf} = \mathbf{f}_d \tag{7.131}$$

we obtain (7.131) as

$$\begin{cases} \mathbf{Ts} + \mathbf{Cd} = \mathbf{f}_s \\ \mathbf{Bs} + \mathbf{Ad} = \mathbf{f}_d \end{cases} \tag{7.132}$$

Assuming that **A** is invertible, the unknown **d** can be eliminated from (7.132) to get a reduced system of equations, and finally to calculate **s**. Therefore

$$\mathbf{d} = -\mathbf{A}^{-1}\mathbf{B}\mathbf{s} + \mathbf{A}^{-1}\mathbf{f}_d \tag{7.133}$$

and, by substitution of (7.133) into (7.132) it is obtained that

$$\left(\mathbf{T} - \mathbf{C}\mathbf{A}^{-1}\mathbf{B}\right)\mathbf{s} = \mathbf{f}_s + \mathbf{C}\mathbf{A}^{-1}\mathbf{f}_d \tag{7.134}$$

The procedure of transformation of (7.133) is called a reduction step – the total number of unknowns is reduced here two times. Let us introduce the following recursions:

$$\begin{cases} \mathbf{K}_0 = \mathbf{K}, \mathbf{f}_0 = \mathbf{f} \\ \mathbf{K}_1 = \mathbf{T}_0 - \mathbf{C}_0\mathbf{A}_0^{-1}\mathbf{B}_0, \mathbf{f}_1 = \mathbf{L}\mathbf{f}_0 + \mathbf{C}_0\mathbf{A}_0^{-1}\mathbf{H}_0\mathbf{f}_0 \end{cases} \tag{7.135}$$

Since that, we obtain

$$\mathbf{K}_1\mathbf{s}_1 = \mathbf{f}_1 \tag{7.136}$$

which is similar to the starting equations where the unknown is given as $\mathbf{s}_1=\mathbf{L}\mathbf{q}$. The process shown above can be repeated up to n times according to the following recursion:

$$\begin{cases} \mathbf{K}_{j+1} = \mathbf{T}_j - \mathbf{C}_j\mathbf{A}_j^{-1}\mathbf{B}_j \\ \mathbf{f}_{j+1} = \mathbf{L}_j\mathbf{f}_j + \mathbf{C}_j\mathbf{A}_j^{-1}\mathbf{H}_j\mathbf{f}_j \end{cases} \tag{7.137}$$

where

$$\begin{cases} \mathbf{T}_j = \mathbf{L}_j\mathbf{K}_j\mathbf{L}_j^T \\ \mathbf{B}_j = \mathbf{H}_j\mathbf{K}_j\mathbf{L}_j^T \\ \mathbf{C}_j = \mathbf{L}_j\mathbf{K}_j\mathbf{H}_j^T \\ \mathbf{A}_j = \mathbf{H}_j\mathbf{K}_j\mathbf{H}_j^T \end{cases} \tag{7.138}$$

It is seen that considering the dimensions of the initial stiffness matrix in the form of $2n$ x $2n$, then repeating the reduction scheme n times, the resulting equation has the single scalar unknown where the general unknown reconstruction scheme is given by the formula:

$$\mathbf{q}^{(2k-1)} = \frac{1}{\sqrt{2}}\left(\mathbf{s}^{(k)} + \mathbf{d}^{(k)}\right) \tag{7.139}$$

$$\mathbf{q}^{(2k)} = \frac{1}{\sqrt{2}}\left(\mathbf{s}^{(k)} - \mathbf{d}^{(k)}\right) \tag{7.140}$$

An analogous situation takes place when **K** is a stochastic linear operator describing the behaviour of some engineering system, **f** is a random external excitation, while **q** represents the random response of the system. Then, using second order perturbation theory, (7.119) can be expanded as follows:

$$\begin{cases} \mathbf{K}^0\mathbf{q}^0 = \mathbf{f}^0 \\ \mathbf{K}^0\mathbf{q}^{,r} = \mathbf{f}^{,r} - \mathbf{K}^{,r}\mathbf{q}^0 \\ \mathbf{K}^0\mathbf{q}^{(2)} = \left(\mathbf{f}^{,rs} - 2\mathbf{K}^{,r}\mathbf{q}^{,s} - \mathbf{K}^{,rs}\mathbf{q}^0\right) Cov\left(b^r, b^s\right) \end{cases} \tag{7.141}$$

where the first two probabilistic moments of the response are calculated as

$$E[\mathbf{q}] = \mathbf{q}^0 + \tfrac{1}{2}\mathbf{q}^{,rs}\, Cov\left(b^r, b^s\right) \tag{7.142}$$

and

$$Cov\left(\mathbf{q}^r, \mathbf{q}^s\right) = \mathbf{q}^{,r}\mathbf{q}^{,s}\, Cov\left(b^r, b^s\right) \tag{7.143}$$

Applying analogous assumptions as previously, i.e.

$$O\left(\mathbf{K}^0\right) = O\left(\mathbf{K}^{,r}\right) = O\left(\mathbf{K}^{,rs}\right) = 2^n;\ n \in N \tag{7.144}$$

we decompose *m*th order displacement vectors $\mathbf{q}^{(m)}$ as

$$\mathbf{s}_k^{(m)} = \frac{1}{\sqrt{2}}\left(\mathbf{q}_{2k-1}^{(m)} + \mathbf{q}_{2k}^{(m)}\right) \tag{7.145}$$

$$\mathbf{d}_k^{(m)} = \frac{1}{\sqrt{2}}\left(\mathbf{q}_{2k-1}^{(m)} - \mathbf{q}_{2k}^{(m)}\right) \tag{7.146}$$

Since the fact, that the matrix M_n consists of the real numbers only, it is defined in exactly the same way. Then, the decomposition of $\mathbf{q}^{(m)}$ into the vectors $\mathbf{s}^{(m)}$ and $\mathbf{d}^{(m)}$ is introduced as

$$\mathbf{L}\mathbf{q}^{(m)} = \mathbf{s}^{(m)} \tag{7.147}$$

and

$$\mathbf{Hq}^{(m)} = \mathbf{d}^{(m)} \tag{7.148}$$

Therefore, full multiresolutional decomposition of up to second order equilibrium equations is carried out as

$$\mathbf{LK}^{(m)}\mathbf{q}^{(m)} = \left(\mathbf{LK}^{(m)}\mathbf{L}^T\right)\mathbf{Lq}^{(m)} + \left(\mathbf{LK}^{(m)}\mathbf{H}^T\right)\mathbf{Hq}^{(m)} = \mathbf{Lf}^{(m)} \tag{7.149}$$

and

$$\mathbf{HK}^{(m)}\mathbf{q}^{(m)} = \left(\mathbf{HK}^{(m)}\mathbf{L}^T\right)\mathbf{Lq}^{(m)} + \left(\mathbf{HK}^{(m)}\mathbf{H}^T\right)\mathbf{Hq}^{(m)} = \mathbf{Hf}^{(m)} \tag{7.150}$$

Denoting further by

$$\mathbf{LK}^{(m)}\mathbf{L}^T = \mathbf{T}^{(m)}, \mathbf{LK}^{(m)}\mathbf{H}^T = \mathbf{C}^{(m)} \tag{7.151}$$

and

$$\mathbf{HK}^{(m)}\mathbf{L}^T = \mathbf{B}^{(m)}, \mathbf{HK}^{(m)}\mathbf{H}^T = \mathbf{A}^{(m)} \tag{7.152}$$

there holds

$$\mathbf{Lf}^{(m)} = \mathbf{f}_s^{(m)}, \mathbf{Hf}^{(m)} = \mathbf{f}_d^{(m)} \tag{7.153}$$

Finally, the reduction equations are obtained as follows:

- zeroth order equations:

$$\begin{cases} \mathbf{T}^0\mathbf{s}^0 + \mathbf{C}^0\mathbf{d}^0 = \mathbf{f}_s^0 \\ \mathbf{B}^0\mathbf{s}^0 + \mathbf{A}^0\mathbf{d}^0 = \mathbf{f}_d^0 \end{cases} \tag{7.154}$$

- first order equations:

$$\begin{cases} \mathbf{T}^{,r}\mathbf{s}^0 + \mathbf{T}^0\mathbf{s}^{,r} + \mathbf{C}^{,r}\mathbf{d}^0 + \mathbf{C}^0\mathbf{d}^{,r} = \mathbf{f}_s^{,r} \\ \mathbf{B}^{,r}\mathbf{s}^0 + \mathbf{B}^0\mathbf{s}^{,r} + \mathbf{A}^{,r}\mathbf{d}^0 + \mathbf{A}^0\mathbf{d}^{,r} = \mathbf{f}_d^{,r} \end{cases} \tag{7.155}$$

- second order equations:

$$\begin{cases} \mathbf{T}^{,rs}\mathbf{s}^0 + 2\mathbf{T}^{,r}\mathbf{s}^{,s} + \mathbf{T}^0\mathbf{s}^{,rs} + \mathbf{C}^{,rs}\mathbf{d}^0 + 2\mathbf{C}^{,r}\mathbf{d}^{,s} + \mathbf{C}^0\mathbf{d}^{,rs} = \mathbf{f}_s^{,rs} \\ \mathbf{B}^{,rs}\mathbf{s}^0 + 2\mathbf{B}^{,r}\mathbf{s}^{,s} + \mathbf{B}^0\mathbf{s}^{,rs} + \mathbf{A}^{,rs}\mathbf{d}^0 + 2\mathbf{A}^{,r}\mathbf{d}^{,s} + \mathbf{A}^0\mathbf{d}^{,rs} = \mathbf{f}_d^{,rs} \end{cases} \tag{7.156}$$

Since that, we derive the reduction equations for the *m*th order of a vector **d** [182]. The process is much more complicated than in the deterministic case. The three up to the second order equation systems are obtained as follows:

- zeroth order equations:

$$\mathbf{d}^0 = \left(\mathbf{A}^{-1}\right)^0 \left(-\mathbf{B}^0\mathbf{s}^0 + \mathbf{f}_d^0\right) \tag{7.157}$$

- first order equations:

$$\mathbf{d}^{,r} = \left\{\left(\mathbf{A}^{-1}\right)^{,r}\left(-\mathbf{B}^0\mathbf{s}^0 + \mathbf{f}_d^0\right) + \left(\mathbf{A}^{-1}\right)^0\left(-\mathbf{B}^{,r}\mathbf{s}^0 - \mathbf{B}^0\mathbf{s}^{,r} + \mathbf{f}_d^{,r}\right)\right\} \tag{7.158}$$

- second order equations:

$$\begin{aligned}\mathbf{d}^{(2)} = \Big\{&\left(\mathbf{A}^{-1}\right)^{,rs}\left(-\mathbf{B}^0\mathbf{s}^0 + \mathbf{f}_d^0\right) + 2\left(\mathbf{A}^{-1}\right)^{,r}\left(-\mathbf{B}^0\mathbf{s}^0 + \mathbf{f}_d^0\right)^{,s} \\ &+ \left(\mathbf{A}^{-1}\right)^0\left(-\mathbf{B}^{,rs}\mathbf{s}^0 - \mathbf{B}^0\mathbf{s}^{,rs} + \mathbf{f}_d^{,rs}\right)\Big\} Cov\left(b^r, b^s\right)\end{aligned} \tag{7.159}$$

Then, the reduced equation has the following form:

- zeroth order

$$\left(\mathbf{T}^0 - \mathbf{C}^0\left(\mathbf{A}^{-1}\right)^0\mathbf{B}^0\right)\mathbf{s}^0 = \mathbf{f}_s^0 - \mathbf{C}^0\left(\mathbf{A}^{-1}\right)^0\mathbf{f}_d^0 \tag{7.160}$$

- first order

$$\begin{aligned}&\left(\mathbf{T}^{,r} - \mathbf{C}^{,r}\left(\mathbf{A}^{-1}\right)^0\mathbf{B}^0 - \mathbf{C}^0\left(\mathbf{A}^{-1}\right)^{,r}\mathbf{B}^0 - \mathbf{C}^0\left(\mathbf{A}^{-1}\right)^0\mathbf{B}^{,r}\right)\mathbf{s}^0 \\ &+ \left(\mathbf{T}^0 - \mathbf{C}^0\left(\mathbf{A}^{-1}\right)^0\mathbf{B}^0\right)\mathbf{s}^{,r} \\ &= \mathbf{f}_s^{,r} - \mathbf{C}^{,r}\left(\mathbf{A}^{-1}\right)^0\mathbf{f}_d^0 - \mathbf{C}^0\left(\mathbf{A}^{-1}\right)^{,r}\mathbf{f}_d^0 - \mathbf{C}^0\left(\mathbf{A}^{-1}\right)^0\mathbf{f}_d^{,r}\end{aligned} \tag{7.161}$$

- second order

$$
\begin{aligned}
&\left(\mathbf{T}^{,rs}-\mathbf{C}^{,rs}\left(\mathbf{A}^{-1}\right)^{0}\mathbf{B}^{0}-\mathbf{C}^{0}\left(\mathbf{A}^{-1}\right)^{,rs}\mathbf{B}^{0}-\mathbf{C}^{0}\left(\mathbf{A}^{-1}\right)^{0}\mathbf{B}^{,rs}-2\mathbf{C}^{,r}\left(\mathbf{A}^{-1}\right)^{,s}\mathbf{B}^{0}\right)\mathbf{s}^{0}\\
&+\left(-2\mathbf{C}^{0}\left(\mathbf{A}^{-1}\right)^{,r}\mathbf{B}^{,s}-2\mathbf{C}^{,r}\left(\mathbf{A}^{-1}\right)^{0}\mathbf{B}^{,s}\right)\mathbf{s}^{0}+\left(\mathbf{T}^{0}-\mathbf{C}^{0}\left(\mathbf{A}^{-1}\right)^{0}\mathbf{B}^{0}\right)\mathbf{s}^{,rs}\\
&+2\left(\mathbf{T}^{,r}-\mathbf{C}^{,r}\left(\mathbf{A}^{-1}\right)^{0}\mathbf{B}^{0}-\mathbf{C}^{0}\left(\mathbf{A}^{-1}\right)^{,r}\mathbf{B}^{0}-\mathbf{C}^{0}\left(\mathbf{A}^{-1}\right)^{0}\mathbf{B}^{,r}\right)\mathbf{s}^{,s}\\
&=\mathbf{f}_{s}^{,rs}-\mathbf{C}^{,rs}\left(\mathbf{A}^{-1}\right)^{0}\mathbf{f}_{d}^{0}-\mathbf{C}^{0}\left(\mathbf{A}^{-1}\right)^{,rs}\mathbf{f}_{d}^{0}-\mathbf{C}^{0}\left(\mathbf{A}^{-1}\right)^{0}\mathbf{f}_{d}^{,rs}\\
&-2\left(\mathbf{C}^{,r}\left(\mathbf{A}^{-1}\right)^{,s}\mathbf{f}_{d}^{0}+\mathbf{C}^{0}\left(\mathbf{A}^{-1}\right)^{,r}\mathbf{f}_{d}^{,s}+\mathbf{C}^{,r}\left(\mathbf{A}^{-1}\right)^{0}\mathbf{f}_{d}^{,s}\right)
\end{aligned}
\tag{7.162}
$$

Since that, the first recursive step for *m*th order stochastic equations is obtained as

$$
\begin{cases}
\mathbf{K}_{0}^{(m)}=\mathbf{K}^{(m)},\mathbf{f}_{0}^{(m)}=\mathbf{f}^{(m)}\\
\mathbf{K}_{1}^{(m)}=\mathbf{T}_{0}^{(m)}-\left(\mathbf{C}_{0}\mathbf{A}_{0}^{-1}\mathbf{B}_{0}\right)^{(m)},\mathbf{f}_{1}^{(m)}=\mathbf{L}_{0}^{(m)}\mathbf{f}_{0}^{(m)}+\left(\mathbf{C}_{0}\mathbf{A}^{-1}\mathbf{H}\mathbf{f}_{0}\right)^{(m)}
\end{cases}
\tag{7.163}
$$

As a result, the triple up to the second order equations for $s_{1}^{(m)}$ are rewritten as follows:

$$\mathbf{K}_{1}^{0}\mathbf{s}_{1}^{0}=\mathbf{f}_{1}^{0} \tag{7.164}$$

$$\mathbf{K}_{1}^{,r}\mathbf{s}_{1}^{0}+\mathbf{K}_{1}^{0}\mathbf{s}_{1}^{,r}=\mathbf{f}_{1}^{,r} \tag{7.165}$$

$$\mathbf{K}_{1}^{,rs}\mathbf{s}_{1}^{0}+2\mathbf{K}_{1}^{,r}\mathbf{s}_{1}^{,s}+\mathbf{K}_{1}^{0}\mathbf{s}_{1}^{,rs}=\mathbf{f}_{1}^{,rs} \tag{7.166}$$

where $s_{1}^{(m)}=Lq^{(m)}$. Repeating this process up to n times, which is possible considering initial dimensions of the matrix $\mathbf{K}$, it is obtained for *m*th order

$$
\begin{cases}
\mathbf{K}_{j+1}^{(m)}=\mathbf{T}_{j}^{(m)}-\left(\mathbf{C}_{j}\mathbf{A}_{j}^{-1}\mathbf{B}_{j}\right)^{(m)}\\
\mathbf{f}_{j+1}^{(m)}=\mathbf{L}_{n-j}^{(m)}\mathbf{f}_{j}+\mathbf{L}_{j}\mathbf{f}_{j}^{(m)}+\left(\mathbf{C}_{j}\mathbf{A}_{j}^{-1}\mathbf{H}_{n-j}\mathbf{f}_{j}\right)^{(m)}
\end{cases}
\tag{7.167}
$$

with

$$
\begin{cases}
\mathbf{T}_{j}^{(m)}=\mathbf{L}_{n-j}\mathbf{K}_{j}^{(m)}\mathbf{L}_{n-j}^{T}\\
\mathbf{B}_{j}^{(m)}=\mathbf{H}_{n-j}\mathbf{K}_{j}^{(m)}\mathbf{L}_{n-j}^{T}\\
\mathbf{C}_{j}^{(m)}=\mathbf{L}_{n-j}\mathbf{K}_{j}^{(m)}\mathbf{H}_{n-j}^{T}\\
\mathbf{A}_{j}^{(m)}=\mathbf{H}_{n-j}\mathbf{K}_{j}^{(m)}\mathbf{H}_{n-j}^{T}
\end{cases}
\tag{7.168}
$$

while the reconstruction scheme for the *m*th order solution vector is given by the following formula:

$$\mathbf{q}_{2k-1}^{(m)} = \frac{1}{\sqrt{2}}\left(\mathbf{s}_k^{(m)} + \mathbf{d}_k^{(m)}\right) \tag{7.169}$$

$$\mathbf{q}_{2k}^{(m)} = \frac{1}{\sqrt{2}}\left(\mathbf{s}_k^{(m)} - \mathbf{d}_k^{(m)}\right) \tag{7.170}$$

Let us consider for illustration the following transformation of the random variables:

$$Y = X^p \cos \omega t \tag{7.171}$$

where $X \in (\Omega, \sigma, P)$, $p \in Z$ and $\omega, t \in \Re$. Therefore, the first two probabilistic moments of *Y* can be calculated as

$$E[Y] = Y^0 + \frac{1}{2}\frac{\partial^2 Y}{\partial X^2} Var(X) \tag{7.172}$$

$$Var(Y) = \left(\frac{\partial Y}{\partial X}\right)^2 Var(X) \tag{7.173}$$

according to the presented second order perturbation technique. It is obtained by the classical differentiation calculus that

$$\frac{\partial Y}{\partial X} = pX^{p-1} \cos \omega t \tag{7.174}$$

and

$$\frac{\partial^2 Y}{\partial X^2} = p(p-1)X^{p-2} \cos \omega t \tag{7.175}$$

The following iterative formula can be proposed for the *n*th perturbation approach:

$$\frac{\partial^k Y}{\partial X^k} = \left[\prod_{l=0}^{k}(p-l)\right] X^{p-(l+1)} \cos \omega t \tag{7.176}$$

Therefore, the expected values are determined

$$E[Y] = E^p[X] \cos \omega t + \frac{1}{2} p(p-1)X^{p-2} \cos \omega t Var(X) \tag{7.177}$$

and variances as

$$Var(Y) = \left(pX^{p-1}\right)^2 cos^2\,\omega t Var(X) \tag{7.178}$$

in the second order perturbation approach. The visualisation of all wavelet functions and their approximations are presented below using the symbolic computation package MAPLE [182]. The following function is used $f(t) = \frac{1}{l(\omega)}\cos(2\pi t)$, $t \in [0,1]$ where $l(\omega)$ belongs to the additional random space with the expected value $E[l]=10$ and the variance equal to $\mathrm{Var}(l)=4$; $p=-1$. The wavelet projection are shown for $n=3,\ldots,6$ in case of the expected values – in Figures 7.54–7.57 and the wavelet approximations for the variance for $n=4,5,6$ are shown in Figures 7.58–7.60.

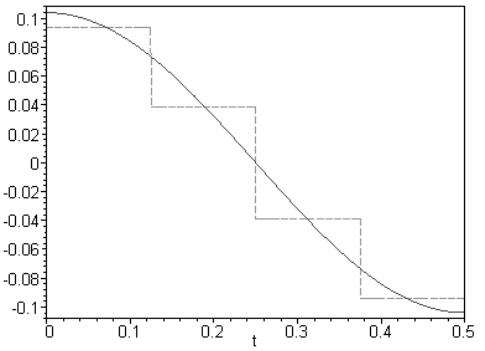

Figure 7.54. Wavelet projection of expected values for $n=3$

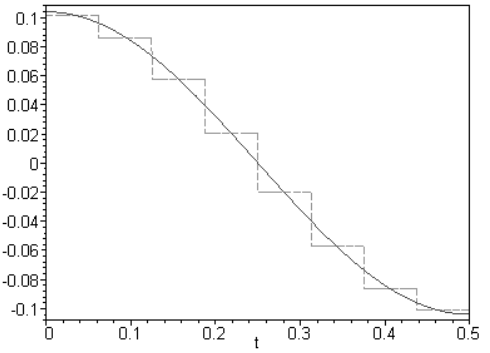

Figure 7.55. Wavelet projection of expected values for $n=4$

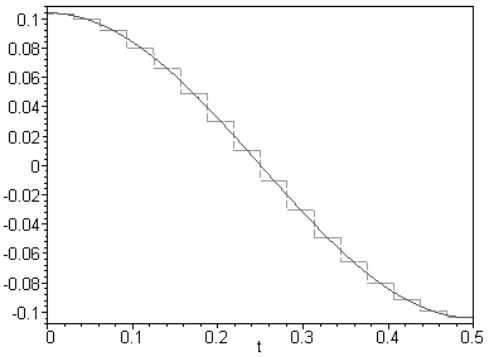

Figure 7.56. Wavelet projection of expected values for n=5

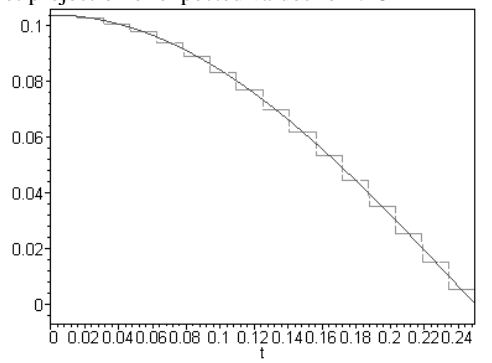

Figure 7.57. Wavelet projection of expected values for n=6

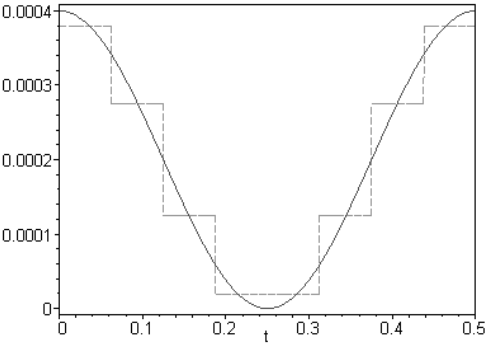

Figure 7.58. Wavelet projection of variances for n=4

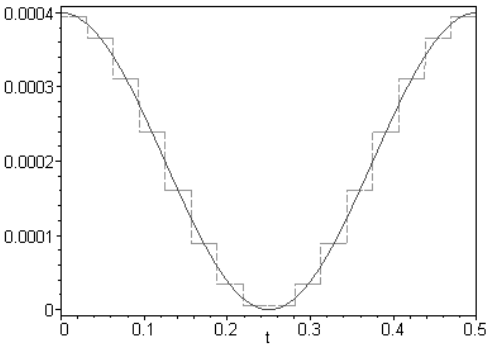

Figure 7.59. Wavelet projection of variances for n=5

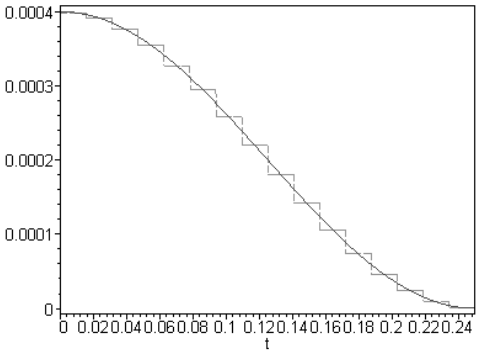

Figure 7.62. Wavelet projection of variances for n=6

The expected values and their wavelet projections are greater than the corresponding deterministic values of $f(t)$ computed for Var(l)=0. Since the expectations and their deterministic origins are very similar, the convergence of analysed projections is quite the same – for n=6 the approximation error on the interval [0,1] in practice can be neglected. The situation changes in the case of variances where projection of the 6^{th} order is not quite smooth; for n=2 cannot be accepted at all because of the constant function resulting from the wavelet projection.

As is documented in Table 7.3, the total computational cost by means of the consumed time and memory necessary to obtain wavelet projection increases nonlinearly together with this projection order. Taking into account that the time of the linear equation system solution shows the same tendency, the very exact solution of (7.120) with 7^{th} and even higher order wavelet projection needs more powerful computers. The last column of the computer test shows that the approximation of variances needs essentially more time and memory than the analogous projection of zeroth order moments (deterministic values) and the expectations (first moments). It should be documented by the relevant numerical tests, if the computational symbolic projection cost increases together with the order of the probabilistic moment being projected onto the same wavelet family.

Table 7.3. Computational cost of wavelet projection (for COMPAQ 475 MHz)

Projection order	q total dimension	f(t) secs/MB	E[f(t)]	Var[f(t)]
2	4	7.4/1.94	8.4/1.94	8.9/2.06
3	8	10.1/2.19	10.9/2.19	11.0/2.31
4	16	14.1/2.62	14.9/2.62	17.3/2.69
5	32	20.7/3.25	25.7/3.31	31.8/3.44
6	64	53.0/4.56	53.7/4.56	70.5/4.94
7	128	131.0/7.06	130.7/7.06	185.4/7.75
8	256	395.3/12.2	360.8/12.2	593.2/13.50

7.8 Concluding Remarks

As was demonstrated above, the wavelet–based multiresolutional computational techniques can be very efficient, considering the capability of heterogeneity analysis on extremely different geometrical scales in the same time. Such phenomena appear frequently in engineering composites – at the interface between the components, on microscale connected with the periodicity cell, for a window on mesoscale for a couple of reinforcing fibres or particles as well as for the macroscale connected with the global composite structure. As can be observed, the wavelet-based numerical methods (especially the Finite Element Method) can be successfully used even for the heterogeneous media with random or stochastic microstructure thanks to implementation of a randomisation method (simple algebra, PDF integration, Monte Carlo simulation, stochastic perturbation or even spectral analyses).

The homogenisation method discussed in this chapter enables us to apply an alternative approach, where the effective material parameters (or its probabilistic moments) are determined first and then the entire composite is analysed using traditional computational techniques. Wavelet-based multiresolutional approach to the homogenisation problem should, however, be formulated to introduce the components characteristics on many scales into the final effective structural parameters. As was demonstrated in the mathematical considerations, homogenised properties in multiscale analysis and classical macro–micro passage are essentially different, even in a deterministic formulation, which was observed previously in three scale Monte Carlo simulation based homogenisation studies for the fibre–reinforced composites [191,197].

Finally, let us note that due to the character of the homogenised 1D elastostatic problem, computational studies on effective coefficient probabilistic behaviour can be applied without any further modifications in the heat conduction problem of a composite with exactly the same multiscale internal structure as well as for any linear field problem with random coefficients defined by their first two

probabilistic moments. The real and imaginary parts of the effective coefficient for the wave equation can be used in acoustic wave propagation in random media. It is observed that for wave propagation, homogenised coefficients strongly depend on the same range on angular velocity and the interrelation of material properties of the layered medium components.

The most important result of the homogenisation–based Finite Element modelling of the periodic composite beams is that replacing the real composite behaviour is very well approximated by the homogenised model response. For a smaller number of bays in the periodic structure, wavelet–based homogenisation gives more accurate results, while the classical approach is more efficient for the increasing number of bays. Maximum deflections of the analysed beams are approximated by all the models with the same precision, which increases for increasing number of bays in the whole structure.

The wavelet–based multiresolutional homogenisation method introduces new opportunities to calculate effective parameters for the composites with material properties given in various scales by some wavelet functions. This method is more attractive from the mathematical point of view. However it is characterised by new, closer bounds on the homogenisability of composite structures, but it eliminates all formal problems resulting from the assumption of small parameter existence between macro– and microscales. Now, practically any number of various scales can be considered in composite materials and structures, which is important in all these cases, where material properties are obtained through signal detection and its analysis. Finally, obtaining satisfactory agreement between the real and homogenised structures enables the application of this method to the forced vibrations of deterministic systems as well as the use of dynamical systems with stochastic parameters.

The second order perturbation wavelet projection gives complicated formulae for approximation of the original functions or matrices, which enables fast wavelet–based discretisation of random variables and/or fields. It is necessary to recall the algebraic restrictions on the first two probabilistic moments of the input to achieve the coefficient of variation to be essentially smaller than 0.15.

However it is documented by the above numerical examples that the wavelet projection of the expected value and its deterministic origin have almost the same character – the same order of approximation is necessary to achieve the same convergence and error level. Wavelet projection of variance (and higher order probabilistic characteristics) needs greater precision, especially for smaller values of the projection order n. Let us note that analogous projection for random functions or operators defined in two– or three–dimensional spaces can be done by the use of Daubechies wavelets in a similar manner to that presented here.

Symbolic computations package MAPLE [61,70] (as well as other numerical tools of this class) is very efficient in wavelet projections of various discrete and/or continuous functions because the efficiency of the projection (and its averaged error) can be recognised graphically in specially adopted plots. Otherwise, a special purpose numerical error routine should be implemented and applied.

The most important result of the homogenisation–based Finite Element modelling of the periodic composite beams is that the real composite behaviour is very well approximated by the homogenised model response. The multiresolutional homogenisation technique giving a more accurate approximation of the real structure behaviour is decisively more complicated in numerical implementation because of the necessity of applying the combined symbolic–FEM approach. A wavelet–based space–time decomposition should be applied in computational modelling of the transient heat transfer problems in heterogeneous media.

Furthermore, mathematical and numerical studies should be conducted to increase nonstationary heat transfer modelling in unidirectional composites by the application of the homogenisation method. In the case of small contrast between heat capacities of the constituents, the method proposed was verified as effective; the situation changes when the value of contrast parameter increases dramatically.